2023

# Neutral And Charged Bis(Triarylamines) For Use In Grid Scale Battery Technologies

Taylor Matthews

*Eastern Kentucky University*, taylormatthews129@gmail.com

NEUTRAL AND CHARGED BIS(TRIARYLAMINES) FOR USE IN GRID SCALE
BATTERY TECHNOLOGIES


BY


TAYLOR MATTHEWS


THESIS APPROVED:


_____
Chair, Advisory Committee

_____
Member, Advisory Committee

_____
Member, Advisory Committee

_____
Dean, Graduate School

STATEMENT OF PERMISSION TO USE

In presenting this thesis in partial fulfillment of the requirements for degree conferral at Eastern Kentucky University, I agree that the Library shall make it available to borrowers under rules of the Library. Brief quotations from the documents are allowable without special permission, provided that accurate acknowledgments of the source is made. Permission for extensive quotation from or reproduction of this document may be granted by my major professor in [his/her] absence, by the Head of Interlibrary Services when, in the opinion of either, the proposed use of the material is for scholarly purposes. Any copying or use of the material in this document for financial gain shall not be allowed without written permission.

Signature:

X _____

Date:  4/10/2022

NEUTRAL AND CHARGED BIS(TRIARYLAMINES) FOR USE IN GRID-SCALE

BATTERY TECHNOLOGIES


BY


TAYLOR MATTHEWS


Submitted to the Faculty of the Graduate School of
Eastern Kentucky University
in partial fulfillment of the requirements for the degree of

MASTER OF SCIENCE

2022

# ACKNOWLEDGEMENTS

I would like to acknowledge and give my thanks to my mentor Dr. Judy Jenkins. Dr. Jenkins has been a pilar of support for my decision to pursue a master's degree and now, a PhD.  As I voiced my uncertainty in either continuing education or research, she always highlighted my strengths and potential by being honest, available, and challenging me even further.

I would also like to give thanks to my thesis committee members, Dr. Abdelhay and Dr. Quan, for their support and suggestions throughout my research project. Lastly, I would like to acknowledge the EKU Chemistry department for allowing students to learn and grow in spaces founded in opportunity.

# ABSTRACT

Energy storage systems allow flexibility in control and maintenance of the electric grid while integrating renewable energy resources to mitigate carbon emissions. Redox flow batteries (RFBs) are stationary energy storage systems that convert chemical energy to electrical energy by charge-transfer reactions. Designing molecules that are capable of stable multi-electron redox reactions per active-species molecule can increase the efficiency of future systems. Spectroelectrochemistry, the combination of spectroscopy and electrochemistry, allows for quantitative and qualitative analyses of electron-transfer processes. The focus of this research is to use optical and electrochemical properties obtained from spectroelectrochemistry to determine the stability of neutral and charge states of a chemical species. Exploring the relationships between molecular structure and stability is essential to the performance of RFBs because this allows for rational design of stable active species.

# TABLE OF CONTENTS

# LIST OF TABLES

# LIST OF FIGURES

# Chapter 1 Introduction and Background

## 1.1 Motivation

The Fourth Industrial Revolution is characterized by the integration of physical, digital, and biological domains. As the revolution is propelled by artificial intelligence, internet of things, robotics, electric unmanned aerial vehicles or drones, 3-D printing, and other digital innovations, the demand for electricity will increase substantially. Worldwide annual electricity production is expected to reach 40,000 terawatt hours in the next 30 years, more than doubling between 2010 and 2050.[1] Current power generation is mostly combustion-based, with over two-thirds of electricity generation from fossil fuels such as coal (42%), natural gas (21%), and oil (5%); the remining power is generated from nuclear (14%), hydro (15%), and renewable energy sources (RES, 3%).[2] For every kilowatt-hour (kWh) of electricity generated by burning coal, 1000 g of carbon dioxide emission is produced; US power plants alone emit 1.5 billion tons of carbon dioxide per year.[2] Burning fossil fuels for electricity is the largest source of greenhouse gas emissions and the main contributor to global warming.[2]

In order to meet these energy needs without further increasing greenhouse gas emissions, energy storage technologies that decarbonize the energy system by storing energy from renewable sources are needed. For instance, if 90% of power generation in existing systems came from non-carbon emitting technologies, carbon dioxide emissions would be reduced from 530 $gCO_2$/kWh to 33 $gCO_2$/kWh.[1] Current clean sources such as hydroelectric, photovoltaics (solar cells, PV), and wind comprise only 3% of the primary power sources in the US.[3] There are also developing technologies in wave, tidal, and biomass energy conversion. However, most RESs are highly intermittent; the peak times of electricity generation and consumer demand often do not coincide. Excess wind energy is lost as customer demand is at its lowest at night when wind generation

is at its maximum. Pumped-storage hydroelectricity has a long service life and high efficiency but has geographical limitations and negative impacts to the environment and ecology. Solar energy is the most abundant RES, the solar radiation energy the Earth receives in 1 hour meets the worldwide energy requirement for a year.[2] However, electricity generation from solar energy fluctuates with location, season, and weather conditions. Successful integration of renewable reliable energy to meet consumers' needs requires cost effective and reliable energy storage at the grid scale, motivating this work.

## 1.2 Grid-Scale Energy Storage

  A viable grid-scale energy storage platform must meet total energy needs, but the electrical load on a power system must also be considered. An electrical load is the component of a circuit that consumes power or energy. Essentially, the electrical energy converted into light, heat, or motion constitutes a load on the circuit (lightbulbs, microwaves, electric fans, etc.). Aggregate electric power load on the grid changes based on consumer needs. For instance, electricity consumption is at its lowest demand at night and at its highest, peak load, during the day. Cycling—switching smaller electricity generating units on and off as a response to changes in the system's load requirements—is used to handle variations in electrical load. Typically, smaller energy sources like steam lines equipped with turbines, generators, and other auxiliary components are used when responding to the increased demand of consumers over short periods of time (100 hours a year or less) because it is difficult to increase or decrease coal-based energy quickly. Though cycling does allow power plants to maintain sufficient supply for varying electrical load, cycling continuously ramps electrical power generation up and down, which ultimately reduces power plant efficiency,

results in higher fuel consumption, and gives rise to higher carbon emissions per kWh. As demand for electricity increases, both base loads and peak loads will increase, requiring more intermittent generation or storage and proportionally increasing carbon emissions. Currently, global energy storage capacity is near 90 GW of the total 2400 GW production, 2.6%.[4] Energy storage systems (ESS) that supplement or even replace combustion-based energy sources are needed to match customer demand including load variability, to allow flexibility in control and maintenance of the electric grid, and to integrate RESs to mitigate carbon emissions.[3]

Energy storage technologies can be classified according to their field of application and power rating. Small-scale systems have a power rating of less than 1 MW and are mainly used in isolated areas, mobile devices, and electrical vehicles. Medium-power systems, 10-100 MW, are used in remote communities or individual electrical systems. Large-scale systems, over 300 MW, are used for peak leveling and power-quality control.[5] Grid-scale energy storage needs to exceed 300 MW and must be highly efficient while storing hours of continuous energy accumulation to be viable. Important grid-scale energy storage systems used to integrate renewable reliable energy and provide reliable energy storage will be discussed in further sections.[6]

The emergence of "smart grids" offers improved grid reliability and utilization. Energy storage systems coupled with smart grids offer real-time load leveling and integration of RESs. The smart grid is a system of electricity transmission/distribution networks that allows two-way digital communication between loads and generation or distribution grids. The system has control, computer, and automation technologies that work with the current electrical grid to respond digitally to the electric demand. Smart grids accommodate the variability in intermittent large-scale RES power production and offer more efficient electricity transmission, faster response times to power disturbances, and reduce peak demand.[2]

Some electrical energy storage systems – redox flow batteries, for instance – solve the challenges of load cycling by decoupling electrical power and energy generation, which eliminates the need to distinguish between peak and baseload generation. Energy is the ability to do work and power is energy per unit time. In the context of a battery, the higher the power, the faster the battery can do work. Energy can be stored when excess power is generated and released during peak loading periods, allowing consumers access to electricity at any time at a lower cost to energy resources. The regulation of the frequency of power generation and short response time to load shifting improves reliability, stability, and cost to both operators and consumers. The integration of storage systems and smart grids could yield a 4% reduction in energy use by 2030, equivalent to elimination emissions of 50 million cars and save $20 billion annually for utility customers.[3] EES system integration would also decrease the need for fossil-fuel-based facilities, reducing emissions if non-emissive energy platforms are used to generate the stored energy. Table 1.1 describes several metrics used to characterize storage technologies such as capacity, efficiency, durability, and cost.

**Table 1.1 Key terms relevant to EES capacity, efficiency, and durability.**

| Term | Definition |
|---|---|
| Current | Flow of electric charge in a circuit. A stream of charged particles moving through an electrical conductor. |
| Voltage | Electric pressure or electric tension from an electrical power source that pushes charged electrons (current) through a conducting loop |
| Energy | Ability to do work |
| Power | Energy per unit time |
| Specific energy (Wh/kg) | Energy per unit mass. |
| Specific power (W/kg) | Power per unit mass |
| Instantaneous power | How much energy can flow into or out of the battery at any given instant |
| Charging | Energy flows into an EES from an external source and is stored |
| Durability/Cyclability | Number of times the energy storage device can be discharged. Expressed as a number of cycles with each cycle comprising of one charging and one discharging phase. |
| Storage capacity (MWh) | Energy available after charging or total energy stored |
| Volumetric Capacity (Ah/L) | Energy available after charging relative to volume |
| Discharging | Energy stored in an EES is released as electrical energy |
| Depth of discharge | Percentage of the battery or amount of energy that has been discharged relative to the total battery capacity |

**Table 1.1 continued**

| Terms | Definition |
|---|---|
| Efficiency | Ratio of released energy to stored energy with instantaneous power as the defining factor |

## 1.3 Emerging Grid-Scale Energy Storage Techniques

ESS can be divided according to application: low-power and medium-power systems for isolated areas, emergency terminals and individual electrical systems, respectively, and large-scale systems for peak leveling in network connections and power-quality control. Small-scale systems include flywheels, chemical energy in secondary batteries, compressed air, hydrogen fuel cells, and supercapacitors. Large-scale systems include thermal energy, chemical energy in flow batteries, or compressed air coupled with liquid or natural gas.[2, 4] A summary of important grid-scale energy storage technologies is provided in Table 1.2, and several of these technologies are discussed in detail.

**Table 1.2 EES capacity, power output, efficiency, and cost comparisons.**

| EES | Capacity (MWh) | Power output | Efficiency (%) | Cost ($/kWh) |
|---|---|---|---|---|
| Flywheel[7] | 0.025 | | 90-95 | 300-25,000 |
| Pumped hydroelectric[4, 7] | | 1000-2800 MW | 65-80 | 1100-2000 |
| Compressed air[4, 7] | 1500 | 10 MW-1 GW | 70 | 120 |
| Sensible heat[8] | 0.001 | 110 MW | 50-90 | 12 |
| Latent heat[8] | | 1.0 MW | 75-90 | 60 |
| Solar fuels[7, 9] | 195 | 1.0 MW | 30 | 0.15-0.20 |
| Supercapacitors[7, 8, 10] | | 0.05-0.1 MW | 90 | 500-3000 |
| Secondary battery – lead acid[7, 11] | 40 | 10 MW | 75-80 | 150 |
| Secondary battery – lithium ion[7, 11] | 193 | 150 MW | 85-100 | 1038-1483 |
| Redox flow battery – vanadium[7] | 6.0 | 4.0 MW | 70-80 | 534-1483 |
| Hybrid redox flow battery – zinc bromine[7] | 4 | 1 MW | 65-75 | 534-1483 |

Mechanical energy storage techniques include flywheel energy storage, pumped hydroelectric storage, and compressed air energy storage. These methods use stored or otherwise unused water, air, or steam to spin a turbine, converting mechanical or kinetic energy into electrical energy, as shown in Figure 1.1.



**Spinning a Turbine**

Water, steam, or air pushes the turbine blades

Discharge = electricity generation:
1. Moving materials—water, steam, air, or combustion gases—push a series of blades to spin a turbine connected to a rotor shaft
2. Moving magnets on rotor generate an electrical field
3. The rotating magnetic field incudes a current in the copper wire and electricity is provided to the grid

Exciter receives DC power supply

Rotor with electromagnets is turned by the shaft

Stationary stator made of coils of copper wire

The turbine consists of the stator and the rotor

**Figure 1.1** Basic components and operation of a turbine generator.

A turbine consists of a stator, coils of copper wire, a rotor, and a series of electromagnetics. The rotor is rotated by moving materials – water, steam, or air –and accelerated by an external electrical input to generate an electric field, converting the stored potential energy in the water (or steam or air) into mechanical energy in the rotor. As the rotor spins within the stator, the rotating magnetic field acts by electromagnetic induction to induce a current in the copper wire, converting the mechanical energy into electrical energy. Electricity generated by turbine generators is supplied to the grid.

Flywheel energy storage uses a flywheel to convert electrical energy to kinetic energy for storage. A flywheel is a solid cylinder with a large rotating mass that acts as a rotor and a motor/generator. The motor accelerates the flywheel by an external electricity input rather than moving materials. The same motor then

acts as a generator to decelerate and discharge the system, converting kinetic energy back to electrical energy for the grid. FES is a small-scale EES with fast charge-discharge cycles, making them most suitable for fast response and short duration applications — switching between power sources, backup storage, and load leveling. FES systems have higher self-discharging rates, up to 20% of stored energy, than other storage mediums. The self-discharge or energy lost during storage limits the storage and usage duration of the technology.[12]

Pumped hydroelectric storage plants generate and store electrical energy by using flowing water to drive a turbine. When the water flows through a turbine as the water is released from a higher reservoir to a lower reservoir, electricity is generated. PHS are charged when electrical energy is used to pump water from the lower reservoir to a higher elevation reservoir, effectively storing electrical energy as potential energy. PHS systems currently have the largest commercially available storage capacity and are capable of meeting current grid-scale storage capacity.[7] However, suitable sites are limited by topographical conditions, require long construction periods, and require a large initial financial investment.[2]

Compressed air energy storage systems use store the potential energy as compressed gas and generate electricity using a turbine generator. Excess energy from the grid is used to power air compressors, which pump ambient air into a pressurized underground storage facility. To discharge the system, the pressurized air is released, heated, and expanded through a turbine generator to generate electricity. CAES systems are a large-scale EES comparable to PHS in bulk energy storage. However, the energy efficiencies of the technology can reach below 45% as a result of heat losses during air compression.[13]

Generally, heat-based ESSs include a concentrated solar (CSP) component and a heat transfer medium, as shown in Figure 1.2.

**Figure 1.2** Layout of a concentrated solar plant (top) and the conversion of heat to electricity (bottom).
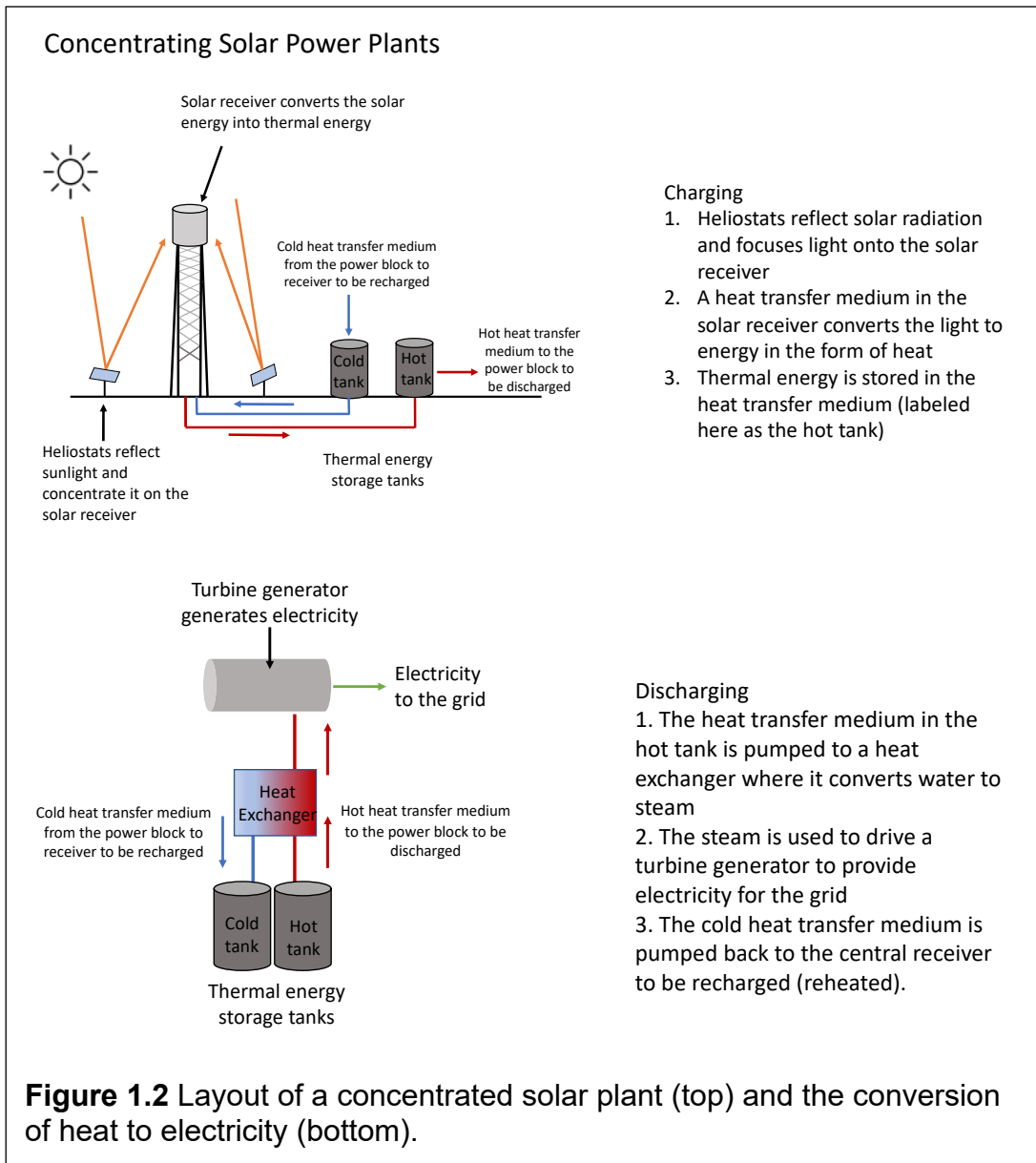
CSP plants use parabolic tracking mirrors to collect solar radiation and to focus light onto either a heat transfer medium - converting energy in the form of light to energy in the form of heat-or a solar panel-converting light to electricity. Electricity generated at CSP plants is used immediately rather than stored. However, thermal energy can be stored using sensible or latent methods.

Sensible heat thermal storage uses a single storage medium and relies on temperature difference of liquid (molten salts) or solid (concrete, rocks) materials to store heat. Using the CSP configuration, a molten salt acts as a

heat transfer fluid. Charging occurs when the molten salt in the receiver is heated by sunlight. The salt is stored in the hot storage tank until discharge. During the discharging process, the hot salt is pumped into the heat exchanger. The stored thermal energy in the hot molten salt converts water to steam, and the steam spins a turbine generator producing electricity. The cooled molten salt is pumped to the cold storage tank and returns to the receiver to be reheated. Alternatively, a solid medium like rocks or concrete can act as both the storage medium and the heat exchanger. The solid material in the solar receiver is heated by solar radiation and a heat transfer fluid, generally water, is passed through the solid to charge and discharge the system.[8] Sensible heat storage systems have demonstrated large energy capacities up to GWh levels but have low energy density, requiring large volumes in order to be efficiently viable at grid-scale. Storage mediums require thermal insulation to mitigate heat losses which increases the cost of the system as it's scaled up.

Latent heat energy storage systems store heat in phase change materials (PCMs) such as paraffin, hydrated salts, and fatty acids. PCMs are embedded with a heat exchanger and stored in a thermal storage block in a one-tank CSP configuration. Heat transfer fluid from the solar receiver, typically water, is circulated through the thermal storage block. The system is charged as the PCM absorbs the latent heat of the water and melts. To discharge, cold water is circulated through the thermal storage block and absorbs the heat as the PCM freezes. The now-heated water boils, and the resulting steam spins a turbine generator.[8] Latent heat energy storage systems have higher energy density relative to sensible storage platforms, but PCMs are expensive, corrosive, and have poor thermal stability, limiting their utility.[14]

Solar energy can also be stored as chemical energy. Solar fuels are produced by water splitting and $CO_2$ splitting (Equations 1.1 and 1.2) using photochemical and photoelectrochemical methods. Photochemical methods use direct solar radiation to drive chemical reactions, forming fuels such as methane from carbon dioxide. Photoelectrochemical methods use solar electricity generated

from a PV for an electrolytic process to yield a fuel. Solar fuels are stored as chemical energy and converted to electrical energy when needed.

Water splitting: $H_2O \rightarrow H_2 + \frac{1}{2}O_2$         (1.1)

$CO_2$ splitting: $CO_2 + 4H_2 \rightarrow CH_4 + 2H_2O$      (1.2)
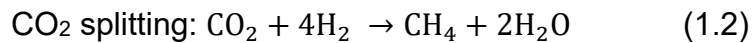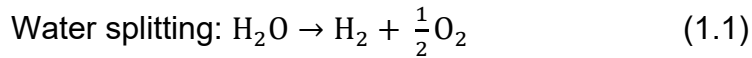
Gases produced by water and $CO_2$ splitting are burned to be used as fuels; burning hydrogen and oxygen gases generates water and burning methane generates carbon dioxide. Using methane as a raw material for other chemical reactions is more advantageous than burning it for energy production. Solar fuel production utilizes renewable and available materials and large-scale power generation has been demonstrated.[7] However, storage technologies are not widely available due to low performance efficiency and high material costs. Solar fuel production utilizing metal oxides and photocatalysts are recent developments but discovering new materials that are low-cost, high-capacity, and environmentally friendly are necessary to move towards widespread commercialization.

Supercapacitors store electrical energy directly by physical separation of charges. Two electrodes separated by an insulator are submerged in an electrolyte. To charge the supercapacitor, a voltage from an external power source is applied between the two electrodes, and electrons and holes accumulate on the anode and cathode, respectively. Electrical energy is stored in the electrical field between the electrodes. The electrodes are then connected as the electrical double layers are released, releasing the accumulated energy as current, discharging the system.[7] Supercapacitors have low energy densities so are most applicable as small-scale systems like portable electronic devices.[10] To be viable at grid-scale, these systems would need to be upscaled which adding to the current high cost, hinders capacitors to be commercialized at the grid-scale.

A fuel cell is an electrochemical device that converts chemical energy from a fuel (hydrogen, natural gas, or methanol) into electricity using an oxidant (oxygen, air, or hydrogen). The fuel and oxidant are consumed and must be continuously fed into the system from an external source.[7] Or, if used as a storage device fuel cells use electricity and water to form hydrogen gas. To discharge a hydrogen fuel cell, hydrogen fuel is oxidized at the anode and oxygen is reduced at the cathode described by the net Equation 1.3. Hydrogen gas is supplied to the anode which acts as a catalyst to break down the hydrogen into protons and electrons (Equation 1.4). The electrons travel an external circuit, providing electricity to the external load. The protons travel through the electrolyte to the cathode where they react with oxygen gas and electrons to produce water and heat (Equation 1.5). The reactions are reversed to charge the system using electricity to form hydrogen gas. Fuel cells reach an energy efficiency of only 60%, requiring a larger amount of energy to be put into the system than what is produced, making them most suitable for small-scale applications.[15]

Net equation: $H_2 + \frac{1}{2}O_2 \rightarrow H_2O_{(l)}$           (1.3)

At the anode: $H_2 \rightarrow 2H^+ + 2e^-$           (1.4)

At the cathode: $\frac{1}{2}O_2 + 2e^- + 2H^+ \rightarrow H_2O_{(l)}$           (1.5)
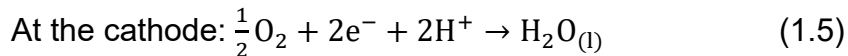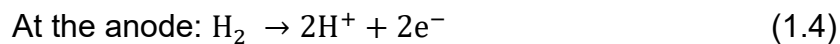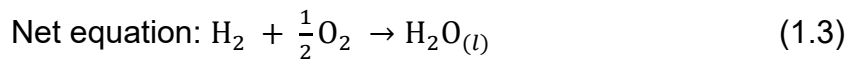
## 1.4 Batteries

A battery can be defined as one or more electrochemical cells that supply electrical energy and can be divided into primary, secondary, and flow systems. A primary battery is assembled charged and designed to be discarded after discharge. Secondary/rechargeable batteries and flow batteries can be recharged by passing current in the reverse direction, ideally returning to the

original charged state. Some of the main secondary and flow battery technologies will be further discussed in detail, as relying on primary batteries for grid-scale energy storage would be prohibitively expensive.

The basic components of a battery are the anode, cathode, electrolyte, redox active species (if the electrolyte is not redox-active), and separator. The anode and cathode, collectively referred to as the electrodes, are charge-transfer mediums and play an active role in the redox reaction. For many battery technologies, the electrodes are submerged in an aqueous electrolytic solution. The electrolyte is an ionic conductor for the movement of redox active species and charge-balancing ions. A separator is placed between the electrodes to prevent them from physically touching. The basic operation of a battery system is shown in Figure 1.3. During discharging, the oxidation reaction at the anode generates electrons which flow through an external circuit (the load). Current suppled to the cathode reduces the species (Equations 1.6 and 1.7). To maintain charge neutrality, cations flow from the anode to pass through an electrolytic solution and separator to the cathode. As the battery is discharged, a continuous flow of charged ions passes through the electrolyte and separator to the cathode and electrons to the external load. Ultimately, work is done in the external circuit (lightbulbs, microwaves, electric fans, etc. come on)

Discharging:

At the anode: $A \rightarrow A^+ + e^-$ $\qquad$ (1.6)

At the cathode: $A^+ + e^- \rightarrow A$ $\qquad$ (1.7)
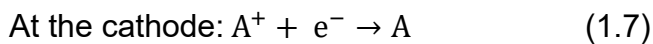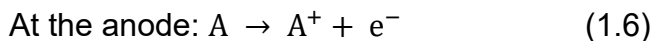
During charging, an electrical charge is supplied by an external power supply and the redox reactions at the electrodes are reversed, reduction occurs at the anode and oxidation occurs at the cathode (Equations 1.8 and 1.9). The positive ions and electrons released by the anode to the cathode move back to the anode, ideally returning the battery to its original state before discharge.

Charging:

At the anode: $A^+ + e^- \rightarrow A$ $\qquad\qquad$ (1.8)

At the cathode: $A \rightarrow A^+ + e^-$ $\qquad\qquad$ (1.9)



**Figure 1.3** A generic secondary battery undergoing discharge (top) and charging (bottom).
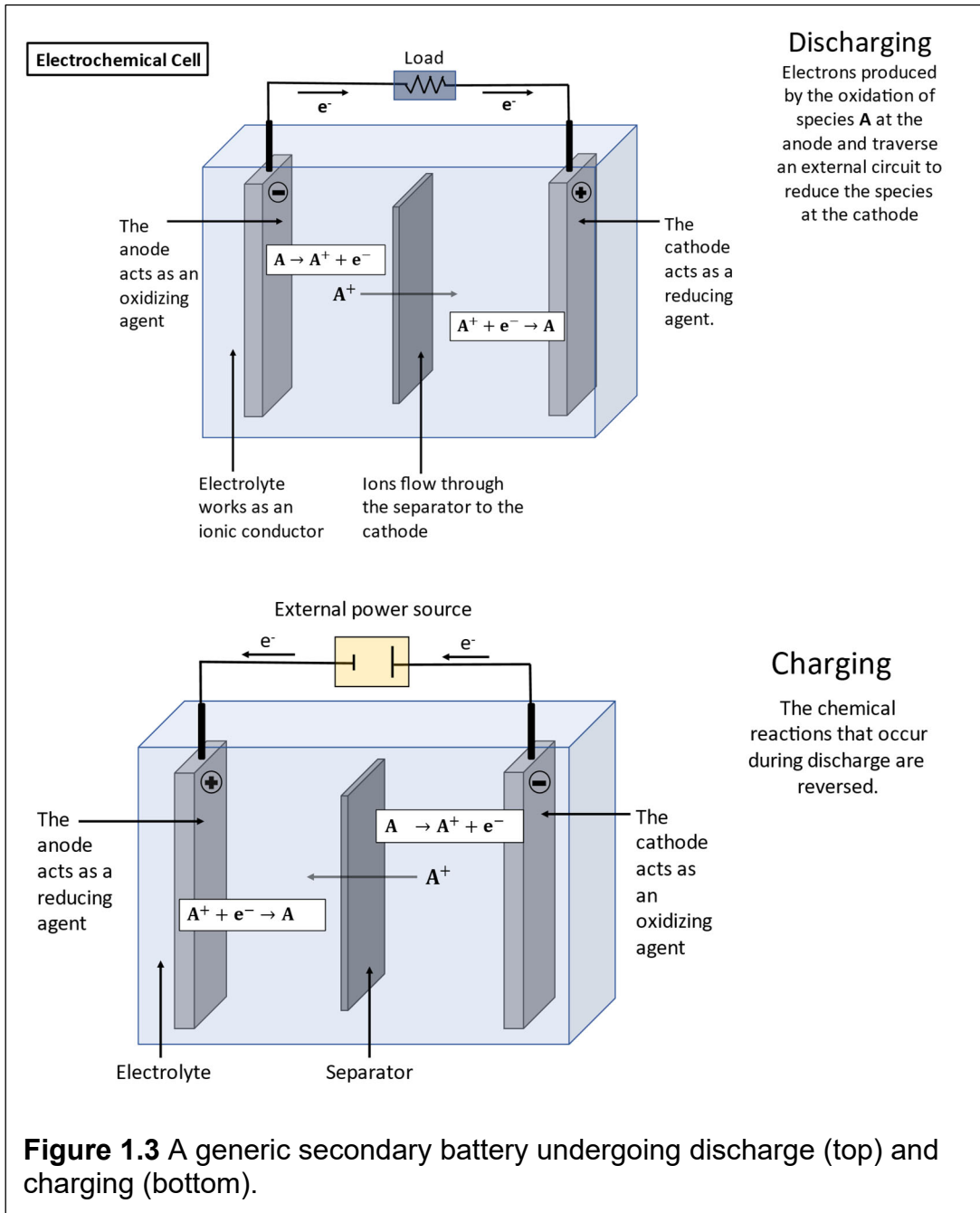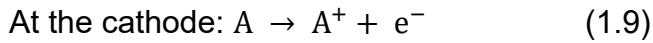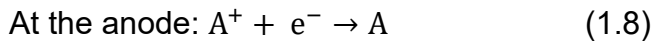
The amount of energy released from a battery can be measured by power output. Power output is expressed in Watt-hours which is the voltage the battery provides multiplied by how much current the battery can provide for an amount of time. Current is the rate at which electrical charge flows and voltage can be thought of as the pressure that causes the charges to flow. The rated current of a battery is the maximum current that can be released from the battery or supplied to the load and is related to the surface area of the electrodes. To increase the rated current, the size of the cell is increased. The output voltage of a battery or voltage released by the cell is determined by the chemistry of the cell. The voltage is the difference between electrochemical potentials of the redox reactions at the electrodes. Electrochemical potentials generally refer to the tendency of the compounds to gain or lose electrons; the strength of the oxidizing and reducing agents are indicated by the magnitude and sign of their potentials. The larger the potential difference between electrodes, the greater the voltage of the cell. To increase the voltage, multiple cells are stacked in a series.

Lead-acid batteries are secondary batteries with a lead anode and lead oxide cathode submerged in an electrolytic solution of water and sulfuric acid. During discharging, lead from the electrodes reacts to form an insoluble lead (II) sulfate layer at the electrode/electrolyte interface (Table 1.3). Lead reacts with hydrogen sulfate ions at the anode to form lead (II) sulfate, hydrogen ions, and electrons.  The hydrogen ions and electrons move to the cathode, the electrons traverse the external circuit and the hydrogen ions move through the electrolyte and separator. At the cathode, lead oxide reacts to form lead (II) sulfate and water.

**Table 1.3 Lead-acid half-cell reactions and corresponding reduction potential during discharge.**

| | Half-cell reduction reaction form: | $E_{red}^0$ (V) |
|---|---|---|
| Cathode | $PbO_{2(s)} + HSO_4^-{}_{(aq)} + 3H^+{}_{(aq)} + 2e^- \rightarrow PbSO_{4(s)} + 2H_2O_{(l)}$ | 1.69 |
| Anode | $Pb_{(s)} + HSO_4^-{}_{(aq)} \rightarrow PbSO_{4(s)} + H^+{}_{(aq)} + 2e^-$ | -0.36 |
| Overall: | $PbO_{2(s)} + Pb_{(s)} + 2H_2SO_4{}^-{}_{(aq)} \leftrightarrow 2PbSO_{4(s)} + 2H_2O_{(l)}$ | 2.05 |

To recharge the battery, the discharge reactions are reversed by applying a voltage from an external power source. Lead oxide is deposited onto the cathode and pure lead is deposited onto the anode, returning the battery to the charged state. A typical single cell lead-acid battery can store 2.1 V and has a capacity of 20 Ah meaning it can deliver 20 A of current in one hour or 1 A for 20 hours. A single cell has a capacity of 40 Wh whilst the largest lead-acid battery installations have a capacity of 40 MWh. Lead-acid batteries are a small-scale EES most suitable for portable devices.[15] Compared to lithium ion and flow batteries, however, lead-acid batteries have the lowest cycling ability because of the corrosion of the electrodes due to sulfation.[2]

Lithium-ion batteries are a secondary battery technology that is currently commercialized for small-scale applications such as portable electronics and electric vehicles. The metal oxide cathode and carbon anode are separated by an electrolytic solution composed of a mixture of lithium salts.[15] During discharging (Table 1.4.), lithium is oxidized at the anode and lithium ions migrate across the electrolyte solution and separator to the cathode. The ions react with the metal oxide at the cathode and electrons from the anode to form a lithium metal oxide. To recharge the battery, the discharge reactions are reversed using energy supplied by an external power source, and lithium ions migrate back to the anode where they are reduced back to neutral lithium and integrated into the carbon anode.

**Table 1.4 Lithium-ion half-cell reactions and corresponding reduction potential during discharge.**

| | Half-cell reduction reaction form: | $E^0_{red}$ (V) |
|---|---|---|
| Cathode | $CoO_{2(s)} + Li^+ + e^- \rightarrow LiCoO_{2(s)}$ | 1.0 |
| Anode | $LiC_6 \rightarrow Li^+ + C_6 + e^-$ | -3.0 |
| Overall: | $CoO_{2(s)} + LiC_6 \rightarrow LiCoO_{2(s)} + C_6$ | 4.0 |

A fully charged lithium-ion battery cell operates at 3.7 V and 2 Ah. The largest installation has a capacity of 193 MWh. Lithium-ion batteries have higher energy densities relative to other rechargeable battery technologies but are at a high risk of overcharge leading to fire hazards.[7] To be viable at the grid-scale, materials to prevent internal over-charge and over-discharge that are cost effective as they are scaled up are necessary.

A redox flow battery (RFB) is a type of rechargeable battery that uses circulating soluble redox couples within an electrochemical cell to store and deliver energy. The electrochemical species are stored in external reservoir tanks and pumped across electrodes that are separated by an ion exchange membrane. The main advantage of RFB systems is the decoupling of power and energy, a characteristic that many of the other EES systems do not have. Additionally, RFBs do not require phase changes (and the corresponding changes in volume) during operation, avoiding some of the problems limiting conventional rechargeable batteries. Vanadium-based RFBs are the most developed flow battery and are commercially available.[16] However, applications for widespread large-scale energy storage are limited due to cost and resource availability. RFBs are a relatively less mature technology and developing a cost-effect system with competitive performance metrics is essential for large-scale utilization. Because the research in this work relates specifically to RFBs, the rest of this chapter will discuss RFBs in more detail.

## 1.5  Redox Flow Batteries

### 1.5.1 Historical Development

The earliest RFB technology was developed in 1884 by Charles Renard to power an air ship and employed a zinc/chloride system and in 1949, the first technology comparable to modern RFBs was patented by Kangro using $Cr_2(SO_4)_3$ as the cathode and anode active material with sulfuric acid supporting electrolyte. Modern RFBs were developed in the 1970s, Lawrence Thaller reported an iron/chromium system solvated in an acidified electrolyte. This system, however, suffered from capacity decay because of electrolyte crossover. To mitigate crossover effects, the vanadium redox flow battery was patented by Skyllas-Kazacos and Robins in the 1980s. Hybrid-flow batteries like Zinc-Bromine were developed by Exxon and Gould Inc. in the 1970's and 1980's, respectively. The iron-chromium, zinc-bromine, and all-vanadium redox flow batteries are either commercially available or under development. Other inorganic redox-active materials have been investigated on a laboratory scale over the last decade.[17]

### 1.5.2 Redox Flow Battery Components

The major advantage of RFBs over the other EES systems is the modular and scalable technology. The independence between power and energy density allows for a flexible design that can easily be cost-effectively scaled up. Long lifetimes, low self-discharge rates, increased safety, and no geographical limitations are also advantageous characteristics of RFBs.  Conventional RFBs have demonstrated MW/MWh energy/power scales, offering promising integration in smart grids and for utilization of intermittent renewable energy. Large amounts of energy can be delivered for long durations in a single discharge cycle, reaching up to 10 hours in some applications.

RFBs are composed of two separated external electrolyte reservoirs and an electrochemical cell. The basic components of a redox flow battery are shown

in Figure 1.4  The electrochemical cell contains two electrolyte half cells, separated by an ion selective membrane. An ion selective membrane is an electrolyte-filled gap or selective membrane, which allows the transport of charge carriers from the supporting electrolyte or counterions of the redox-active species to cross from one half of the electrochemical cell to the other, maintaining electroneutrality and electrolyte balance.[18] Redox-active molecules are dissolved in liquid supporting electrolytes and stored in the electrolyte reservoirs. Together, the redox-active species, electrolyte, and solvent (if applicable) used on the anode side are called the "anolyte." The redox-active species, electrolyte, and solvent (if applicable) on the cathode side is called the "catholyte". Electrodes within the half-cells are generally composed of graphite- or other carbon-based materials. The electrodes are submerged in the electrolyte solutions and connected to current collectors. Current collectors work as electrical conductors to direct the flow of current between electrodes and external circuits. The anolyte and catholyte solutions are pumped from the reservoirs and through the electrochemical cell during the charging and discharging processes such that chemical energy being stored in the external



**Figure 1.4** A generic redox flow battery undergoing discharge.
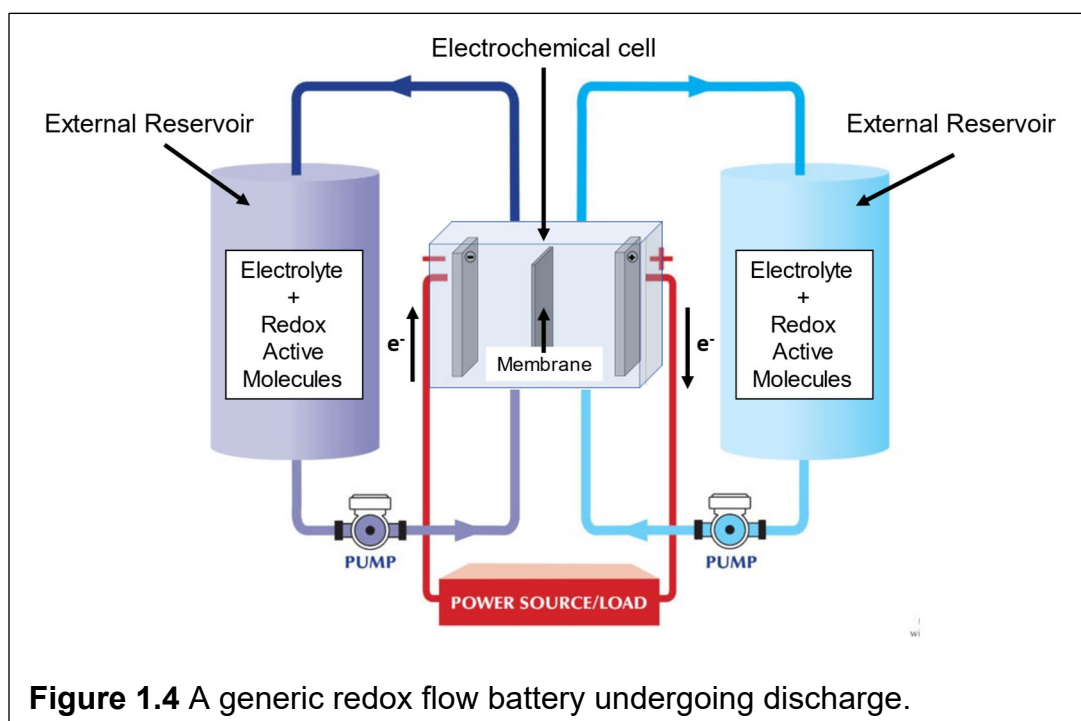
reservoirs is converted to electrical energy by charge-transfer reactions at the electrodes (and vice versa).[19]

During the charging process, an external electrical power source supplies electrical energy to charge the RFB. At the molecular level, the oxidation reaction occurs at the cathode, yielding an electron which is drawn off by the conductive electrode and transferred into the outer circuit. Simultaneously, the transport of charge carriers through the IEM occurs to provide charge balance to the opposite half-cell and the electrons which have travelled the external circuit reduce the second anolyte at the anode. Charging continues until the battery reaches storage capacity which is limited by the amount of redox active materials available. Chemical energy is stored in the anolyte and catholyte until needed. During the discharging process, chemical energy in the anolyte and catholyte are converted to electrical energy, which is transmitted through the external circuit, providing power output to the external load. At the molecular level, oxidation occurs at the anode, yielding one electron for every redox-active species which carries electrical energy. The charge carriers are again transported through the IEM, balancing the opposite half reaction, and reduction occurs at the cathode. The anolyte and catholyte deliver electrical energy until the anolyte and catholyte within the two tanks are completed discharged.

The separation of redox-active materials (stored in reservoirs) and the electrochemical reactions (occurring in the electrochemical cell) decouples the power generation and energy capacity allowing for flexible and tunable stationary applications. Multiple cells can be stacked in a series of increasing voltage and in a bipolar fashion so that current flow from one cell to the next. The energy capacity can be increased by increasing the size of the reservoirs or the concentration of the electrolyte, and power can be increased by increasing the number of cells in a stack or optimizing parallel or series configurations.

Zinc-bromine redox flow batteries (ZBFBs) are a type of hybrid redox flow battery that use metal stripping and plating reactions on one electrode and soluble flowing electrolyte on the other. ZBFBs are considered a hybrid system

because the relationship of power/energy for ZBFBs is more fixed relative to traditional RFBs. The available energy is dependent on the electrode area available for zinc plating. The carbon-based electrodes are submerged in a chloride-based supporting electrolyte and separated by a microporous plastic film.[20] During discharging as shown in Table 1.5., the zinc plated on the anode is oxidized to zinc ions and dissolved into the aqueous anolyte. The electrons reduce the bromine molecules to bromide ions at the cathode. Complexing agents are used to minimize the evolution of bromine. To recharge the battery, the reactions are reversed. Metallic zinc is reduced and plated as a thick film on the anode and bromide ions are oxidized to bromine at the cathode.

**Table 1.5 ZRFB half-cell reactions and corresponding reduction potential during discharge.**

| | Half-cell reduction reaction form: | $E^0_{red}$ (V) |
|---|---|---|
| Cathode | $Br_{2\,(aq)} + 2e^- \rightarrow 2Br^-_{(aq)}$ | 1.08 |
| Anode | $Zn_{(s)} \rightarrow Zn^{2+}_{(aq)} + 2e^-$ | -0.76 |
| Overall: | $Zn_{(s)} + Br_{2(aq)} \rightarrow 2Br^-_{(aq)} + Zn^{2+}_{(aq)}$ | 1.85 |

Complexing agents reduce the evolution of bromine to prevent the high toxicity of the species. Zinc metal has a large volumetric capacity (5854 Ah/L), offering larger energy densities relative to all-vanadium RFBs.[21] ZBFBs provide a high voltage of 1.85 V, 70-75% efficiency, and a specific energy of 65 Wh/kg. They also utilize abundant, low-cost materials in chemical reactions that are highly reversible.[2] These battery systems are optimal for long-term energy storage because they have a lifetime of up to 2000 cycles and has a storage capacity of 500 kWh.[11] The main disadvantages of ZBFBs are the material corrosion, dendrite formation leading to electrical shorting, and high self-discharging rates of 12-15% per month.[3]

All-vanadium redox-flow batteries (VRFBs) are the most developed flow battery systems and are currently commercially available.[19] The battery uses vanadium ions on both sides, with $V^{2+}/V^{3+}$ redox reactions in the anolyte and $VO_2^+/VO^{2+}$ reactions in the catholyte. The use of a single element decreases cross-over effects and allows restoration of capacity by mixing the electrolyte species, increasing long-term cycling, and decreasing required maintenance. Cross-over is the cross-contamination of the anolyte and catholyte through the separator. Mixing anolyte and catholyte varies electrolyte volumes in the external tanks and could result in irreversibly consumed redox-active species. Crossover effects lead to decreased capacity and efficiency of the battery. VRFBs mitigate efficiency losses by regenerating anolyte and catholyte species electrochemically.[3] The ions are dissolved in a sulfuric acid supporting electrolyte and porous carbon fiber-based electrodes are most commonly used. During discharging, oxidation occurs at the anode and reduction occurs at the cathode as shown in Table 1.6. To recharge the battery, the reactions are reversed, oxidation occurs at the cathode and reduction at the anode.

**Table 1.6 ZRFB half-cell reactions and corresponding reduction potential during discharge.**

| | Half-cell reduction reaction form: | $E^0_{red}$ (V) |
|---|---|---|
| Cathode | $VO_2^+ + 2H^+ + e^- \rightarrow VO^{2+} + H_2O$ | 0.99 |
| Anode | $V^{2+} \rightarrow V^{3+} + e^-$ | -0.26 |
| Overall: | $V^{2+} + VO_2^+ + 2H^+ \rightarrow VO^{2+} + V^{3+} + H_2O$ | 1.25 |

VRFBs provide energy densities of 10-20 Wh/L, specific energies of 10-20 Wh/kg, and specific powers of 1-4 W/kg.[18] The largest energy capacity demonstrated is 1.5 MW with an efficiency of 85% and a lifetime of up to 10,000 cycles. ZBFBs offer larger energy densities but VRFBs have a lower self-discharge rate of 5-10% per month, increasing the lifetime significantly and

decreasing the cost of maintenance.[7] The main disadvantage of this battery system is the high cost, instability, and toxicity of active materials. Vanadium-based compounds also have low solubility, as a result of low ion concentrations (2M or less), which limits energy density. [21]

Low-cost RFB systems capable of storing large quantities of energy with efficient performance are essential to wide-scale commercialization of RFBs. The performance of RFBs is dependent on thermodynamics and reflected by redox potentials, mass transport of redox-active species, and electron transfer rates. Redox-active species, electrodes, separators, and cell configurations are factors influencing the promise of these systems. High surface area electrodes with higher electrocatalytic activity that can increase the volume of production of active materials and separator materials with improved selectivity and stability at lower costs that can maximize power and energy densities may afford improvements.

Traditional metal-based RFBs are relatively established technologies although their applications for large-scale energy storage face some drawbacks including expensive and resource-limited active materials, corrosive and hazardous electrolytes, low current performance, electrolyte crossover, and expensive system costs.[22] To address some limitations faced by inorganic RFBs, organic RFBs (ORFBs) synthesized using abundant and low-cost materials offer promising alternatives.

In addition to the general features of existing RFB systems, ORFBs can be low-cost in large-scale applications and synthetically tuned.[22] In addition, the possibility of organic redox species is numerous relative to the limited number of inorganic redox couples.[19] Organic redox-active species are in early stages of development, however a chemical cost of \$27 kW h$^{-1}$ has been demonstrated – a third of the cost of VRFB electrolytes (\$81 kW h$^{-1}$).[19] However, ORFBs have limited cycling performance (typically 100 cycles or less) which has been attributed to electrochemical and chemical instability of redox-active and electrolyte materials.[22]

ORFBs can be divided based on solvent used in electrolytes – aqueous ORFB (AORFB) and nonaqueous ORFB (NAORFB). AORFB are further divided into acidic, neutral, and alkaline systems based on electrolyte pH and NAORFB into all-organic, hybrid organic-metal, and redox-targeting flow batteries based on redox materials. AORFB are the most promising system at present for low-cost, safe, large-scale EES. Water and simple inorganic supporting electrolytes are inexpensive, typically nonflammable, and highly conductive. The main limitation of AORFB systems is low energy densities. [23]

The main advantage of non-aqueous electrolytes is a broader electrochemical window (wide potential range up to 4.0 V) which offers high energy densities. Greater diversity, availability, and tunability of redox-active molecules and redox potentials are other advantageous features of NAORFBs.[24] One major limitation of NAORFBs is lack of high-performance IEM materials. Separators and IEM materials in nonaqueous electrolytes have demonstrated high cell resistance, electrolyte crossover, and side reactions which lead to poor cycling performance. Another limitation is low current and power densities because of low ionic conductivities and high viscosities of nonaqueous electrolytes. At the present stage, NAORFBs fit long-term energy storage demands where high current and power performance are not required.[24]

Limitations caused by electrochemical and chemical instability can be mitigated by designing stable redox-active species. Structural tuning of redox-active molecules has the promise of tailoring reduction potentials, improving solubility, and offering multiple electron transfers (expanding cell voltage to improve energy density). Ideal redox molecules for RFB application should be highly soluble (increasing capacity and energy density), demonstrate fast kinetics (increasing voltage and power density), have highly positive or negative potentials (increasing voltage, energy density, and power density), environmentally conscious, and low cost. A deeper understanding of the solution chemistry and electrochemistry of ORFBs is necessary to further optimize flow battery systems and improve molecular designs.

Our approach is to utilize low-cost redox couples with multiple electron transfers to extend the potential gap, increase output voltage, and improve energy density. The stability, kinetics, and charge-transfer mechanisms of a redox-active species are important to determine before integrating into large-scale systems. This project focuses on analyzing structure property relationships of two-electron transfer organic molecules for use in ORFBs.

# Chapter 2 Materials and Methods

## 2.1  Materials

  Molecules (**1**), **(2)**, and **(3)** were synthesized by the Odom group using a previously reported synthesis. Tetrabutylammonium tetrafluoroborate (TBABF$_4$, 99%) and tetrabutylammonium hexafluorophosphate (TBAPF$_6$) were purchased from Sigma Aldrich and recrystallized from ethanol prior to use. Dichloromethane (DCM, 99.9%) was purchased from Acros Organics and used without further purification. Tris(4-bromophenyl)ammoniumyl hexachloroantimonate (magic blue) was purchased from and tris(2,4-dibromophenyl)amine (magic green) was purchased from Sigma Aldrich and used without further purification. Ferrocene was purchased from Alfa Aesar and used without further purification.  The overarching goal of this work is to determine how the structural differences of molecules **1**, **2**, and **3** impact the properties of these molecules. Because these molecules are candidates for use in redox flow batteries, properties of interest include the redox potentials of the species as well as the stabilities of the neutral and charged species. As such,

the characterization techniques employed and discussed here in detail include spectroscopy, cyclic voltammetry, and spectroelectrochemistry



**Figure 2.1** Chemical structures of Molecules (**1**), (**2**), (**3**), Magic Blue, and Magic Green.
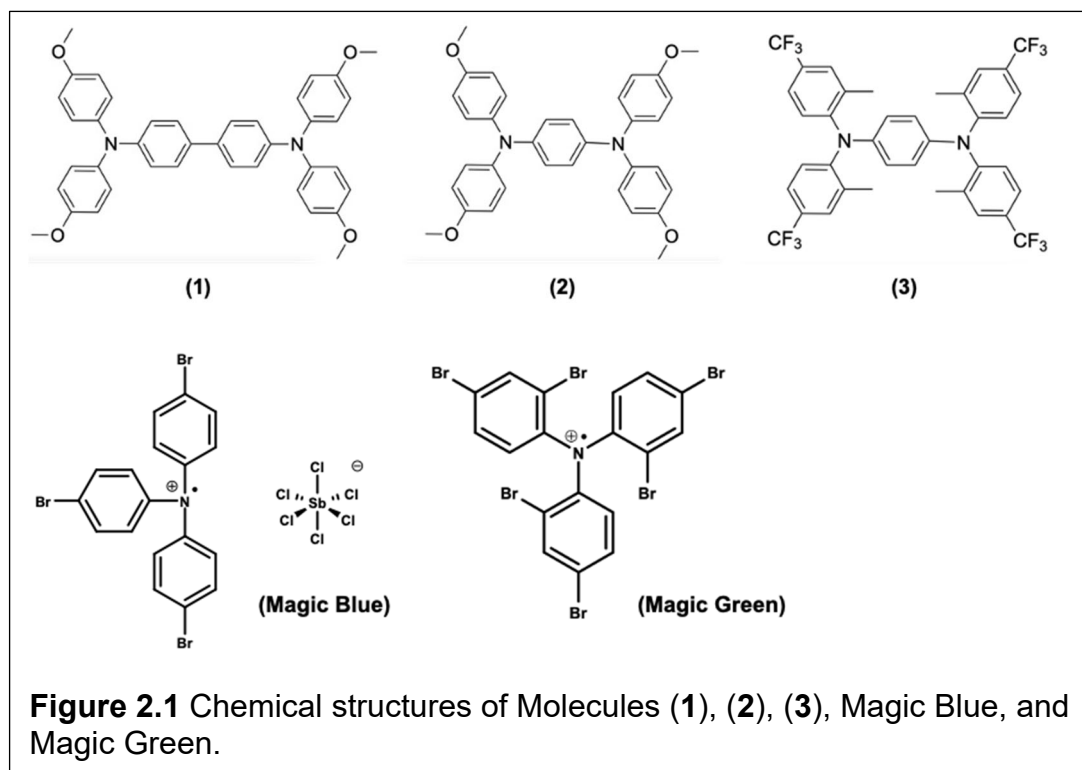
## 2.2 Spectroscopy

Spectroscopic measurements were completed using two different UV/Vis absorbance spectrophotometers, an Agilent 8454 diode array instrument and an Agilent Cary 60 UV-Vis spectrophotometer. A quartz cuvette (10 mm) and the Pine spectroelectrochemical cell (1 mm, part number AKSTCKIT3) were used to collect spectroscopic measurements.

## 2.2.1 Theory of UV-Vis Absorbance Spectroscopy

Chemical compounds can absorb, transmit, emit, or reflect light (photons). Spectroscopy is the measurement and analysis of interactions between electromagnetic radiation – photons – and matter. For many small molecules, electronic transitions between valence orbitals correspond to the energy of light in the UV-visible region of the electromagnetic spectrum, so electronic transitions between energy states of a chemical species can be detected and quantified by monitoring photon absorption or emission. Absorption methods measure the energies of the photons absorbed by the analyte species in the excitation process. The analyte is in its lowest-energy or ground state prior to the application of the external photon energy. As the energy is applied, the species absorbs photons and electrons are promoted temporarily to higher-energy or excited states as shown in Figure 2.2.[25]

The generic absorbance spectrophotometer shown in Figure 2.3 produces, disperses, and measures light. A lens focusses a beam of photons from a light source to a monochromator. The monochromator separates component wavelengths using optical dispersion by refraction using a prism or diffraction



**Figure 2.2** Jablonski diagram for a generic species showing electronic absorption, vibrational, and rotational transitions.
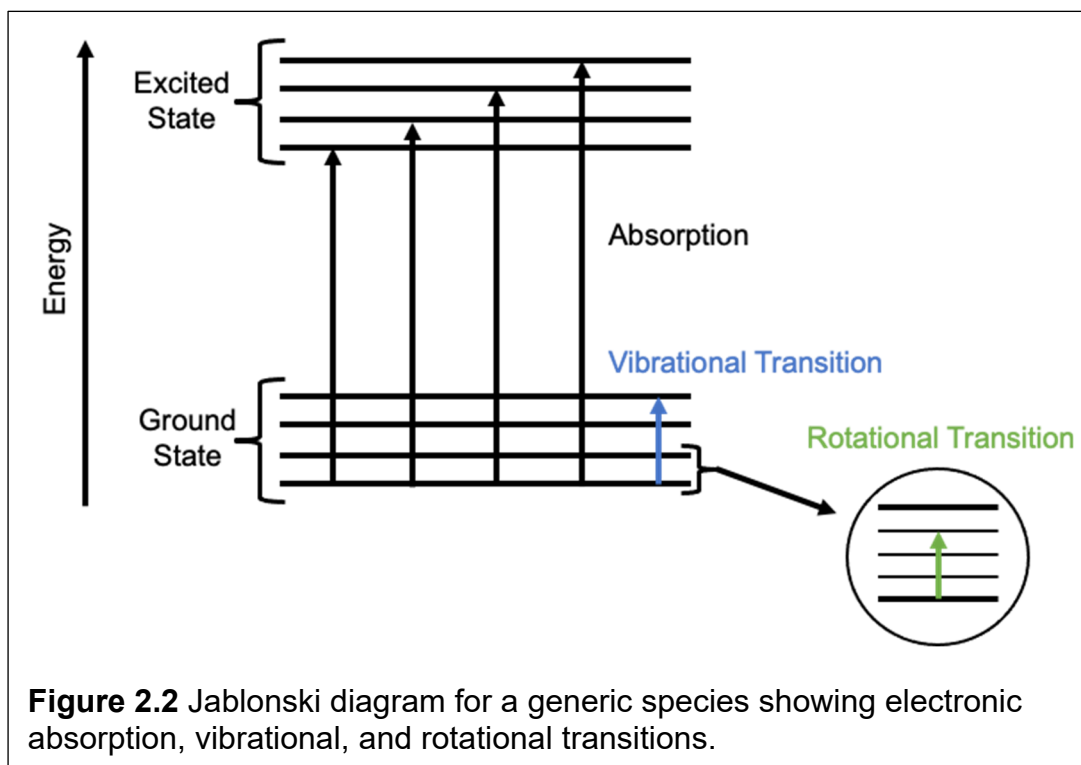
using a diffraction grating. The wavelength selector transmits the desired wavelengths. The light that is not absorbed by the sample will pass through the sample to the detector. A range of photon energies can be collected by selecting different wavelengths sequentially by rotating the prism or grating so that the next band passes through the wavelength selector.[25]



**Figure 2.3** Basic components of a UV-Vis absorbance of spectrophotometers
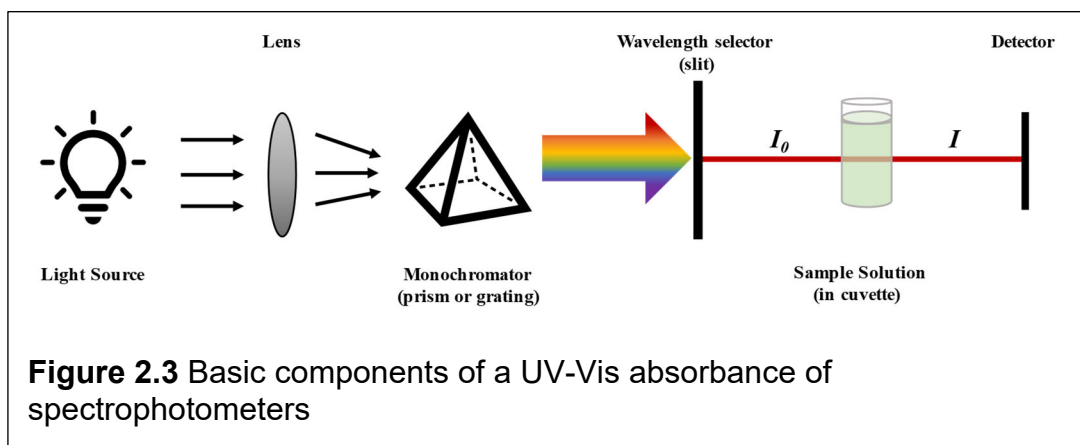
As shown in Equation (2.1), transmittance, $T$, is the fraction of incident light that passes through the sample:

$$T = \frac{I}{I_0} \qquad (2.1)$$

where $I_0$ is the intensity of incident light entering the sample and $I$ is the intensity of incident light passing through the sample to the detector. Functionally, $I_o$ is measured as the photons reaching the detector after passing through a blank, usually a cuvette filled with the solvent only, while $I$ is measured as the photons reaching the detector after passing through a cuvette filled with the solvent and analyte. Absorbance, $A$, is the quantity of light absorbed by a solution and is related to transmittance as shown in Equation (2.2):

$$A = -\log T = -\log \frac{I}{I_0} \qquad (2.2)$$

Generally, data are plotted as absorbance (AU) versus wavelength (nm). The measured absorbance is directly proportional to the concentration and path length as described by the Beer-Lambert law, Equation (2.3),

$$A = \varepsilon \cdot b \cdot c \qquad\qquad (2.3)$$

where $\varepsilon$ is the molar absorptivity coefficient or a measure of the probability of an electronic transition, $b$ is the path length of light through the sample, which is functionally the width of the cuvette, and $c$ is the analyte concentration.

For this project, two types of spectrophotometers were used, an instrument equipped with a Czerny-Turner monochromator and photomultiplier tube (PMT-based) and a diode array instrument. These instruments differ in the energies of light incident on a sample at any given time and in type of detector. A PMT-based spectrophotometer measures how many photons pass through a sample solution at one wavelength (Figure 2.4.). Radiation from a light source is focused to a monochromator where is it dispersed into packets of individual wavelengths. A single wavelength, $I_0$, is selected to pass through the sample and incident light passing through the sample, $I$, enters the PMT. The photons entering the PMT are absorbed and converted to primary electrons, which are then emitted by a photocathode. Ideally, one transmitted photon results in one primary electron. Electrons are accelerated and focused by a focusing electrode to a dynode where they are multiplied (secondary electrons). The secondary electrons are accelerated through a series of dynodes to further multiply the number of electrons corresponding to the transmitted photons in a cascading process generating a large current, ultimately collected by the anode.[26] The current magnitude is proportional to the number of transmitted photons. This process is repeated at each wavelength for both the blank and the sample to obtain $I_0$ and $I$, respectively. The current magnitudes collected by the anode are stored, and the spectrophotometer software converts these values to absorbance according to Equation 2.2.
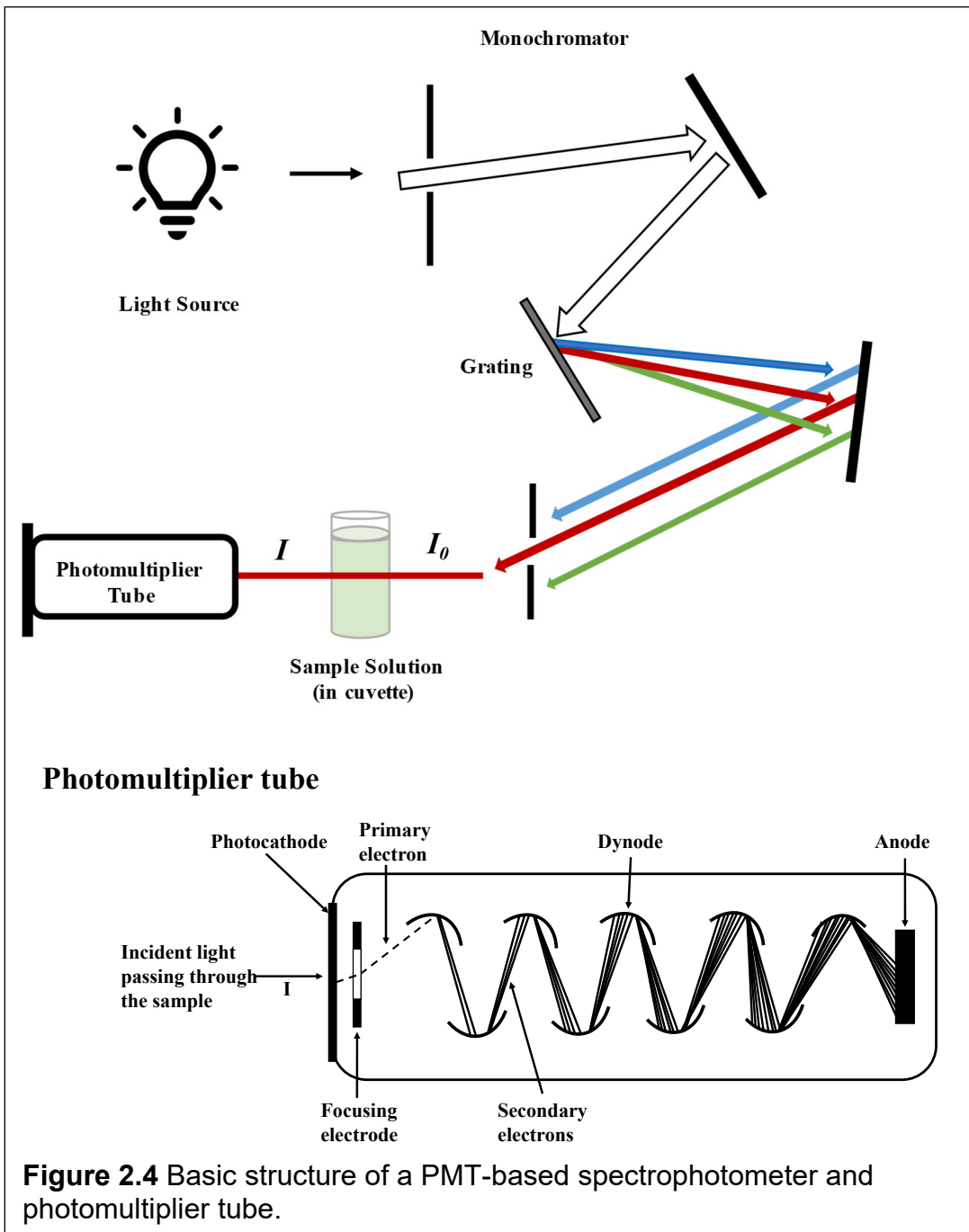
**Figure 2.4** Basic structure of a PMT-based spectrophotometer and photomultiplier tube.

A diode array spectrophotometer measures how many photons pass through a sample solution at multiple wavelengths simultaneously. A diode array detector consists of a series of adjacent photosensitive diodes (Figure. 2.5) Photons from a light source pass directly through the sample before reaching a diffraction grating. The photons are dispersed by the diffraction grating and directed to the photodiode array where photon intensity is measured for each wavelength of dispersed light. Each photon reaching the diode array is converted to an electron, and current measurements for the blank and the sample are converted to absorbance according to Equation 2.2.[25] A PMT-based detector can measure relatively small amounts of radiation because of the amplification process but stray radiation can also amplify, leading to large signal-to-noise ratios. Diode array detectors obtain information over a wide range of wavelengths simultaneously, scanning an entire spectrum in less than one second. However, diode array detectors are less sensitive relative to PMT-based detectors.[27]



**Figure 2.5** Basic figure of a diode array spectrophotometer.
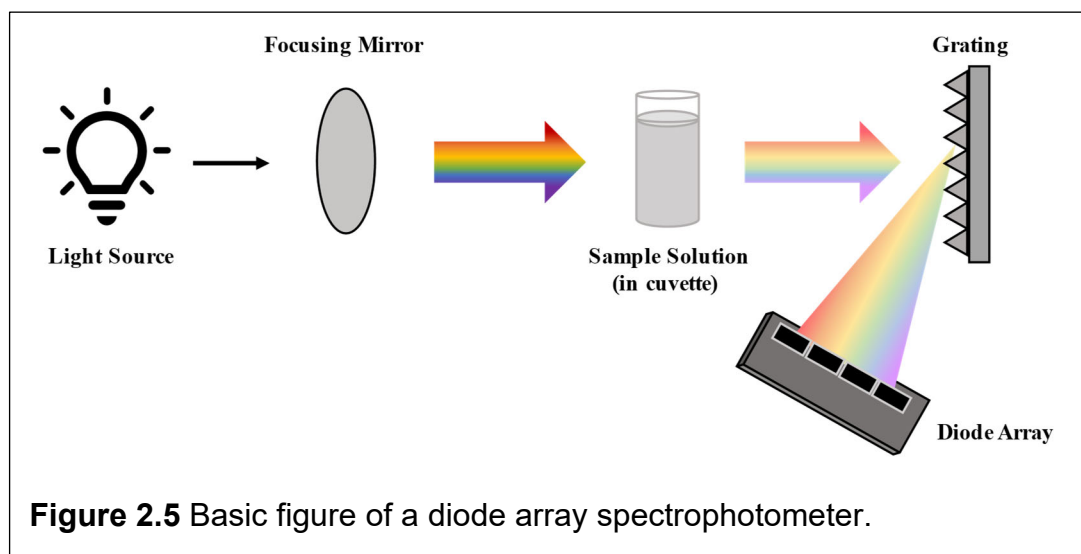
## 2.2.2 Relating absorption spectra to molecular properties

Small organic molecules absorb radiation (light) in different regions of the electromagnetic spectrum, thus an absorption spectrum of an organic molecule can provide several different types of information about the molecule. Generally, an absorption spectrum for an organic molecule consists of one or more bands (peaks). The wavelength of an absorption band is inversely proportional to the energy required to promote an electron from one orbital or state to a higher energy state; electronic transitions requiring relatively more energy occur at shorter wavelengths. Each electronic transition is accompanied by rotational and vibrational transitions that broaden the absorbance band. The energies and numbers of bands observed in a spectrum are related to the electron configuration of the molecule, and the intensity of each band depends on the allowed-ness of the transition.

Many organic compounds are colorless in solution because the energy difference between the sigma-like HOMO and the unoccupied orbitals are larger than the energy of photons in the visible region of the electromagnetic spectrum. However, molecules with pi-conjugated systems, where the highest energy occupied orbitals are pi-like in character, have orbitals separated by smaller energy gaps, corresponding to ultraviolet and visible light. The absorption spectra collected using UV-vis spectroscopy provides information on the extent of conjugation and corresponding molecular structures. As conjugation increases, absorption peak wavelengths tend to shift bathochromically (toward longer wavelengths) because the gaps between the energy levels decreases, requiring less energy to promote electrons. The relative magnitude of the peaks in a given spectrum is related to the molar absorption coefficient, which tends to increase with conjugation length. The molar absorptivity roughly doubles with each conjugated double bond, technically described as a hyperchromic shift in absorption. Changes in the absorption spectra may be observed after oxidation because loss of one or more electrons may change one or more of the following molecular characteristics: bond lengths, orbital energies, the extent of electronic

34

delocalization in the molecule, the number of electronic transitions, and the allowedness of electronic transitions.

In this work, UV-Vis absorbance spectroscopy was used to characterize the neutral, cationic, and dicationic species of molecules 1-3 and to quantitatively assess the stabilities of the neutral, cationic, and dicationic species in various device-relevant environments. Further relationships between absorbance spectra and molecular properties will be discussed in Results and Discussion

## 2.3 Electrochemistry

Cyclic voltammetry experiments were performed in an electrochemical cell (Fig. 6, left) and electrochemical measurements were completed using a CHI 760e bipotentiostat. Cyclic voltammograms were measured using a Pine low-volume electrochemical cell with a ceramic screen-printed electrode. A three-electrode setup was used for experiments, including a working electrode (WE), counter electrode (CE), and a reference electrode (RE Fig. 2.6, right). Though an Ag|AgCl RE was used for data collection, cyclic voltammograms of ferrocene
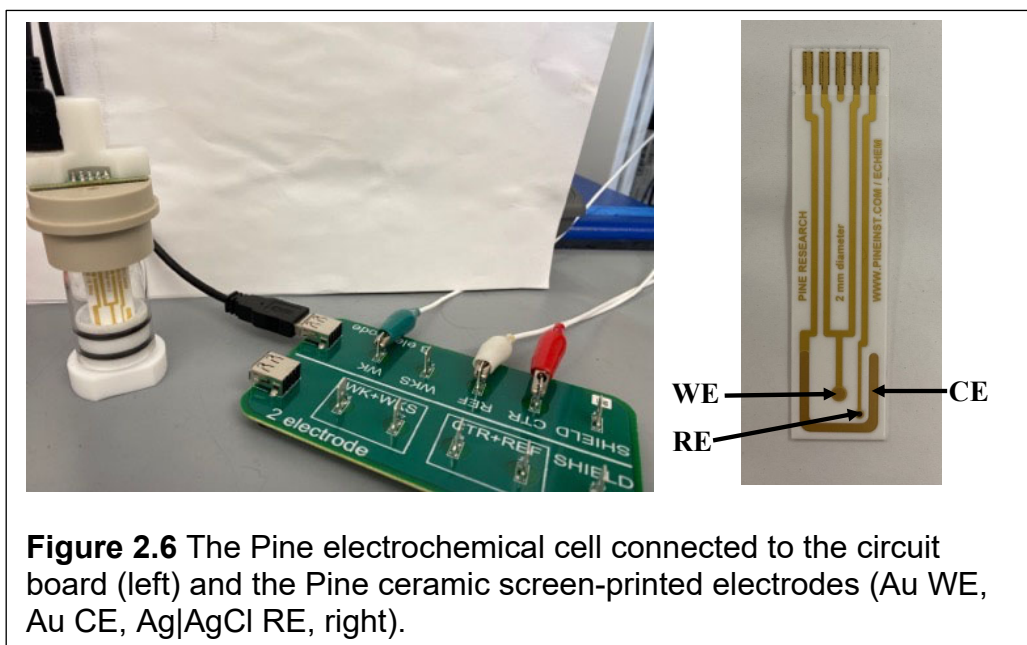


**Figure 2.6** The Pine electrochemical cell connected to the circuit board (left) and the Pine ceramic screen-printed electrodes (Au WE, Au CE, Ag|AgCl RE, right).

(Fc) were collected, and all potentials are reported here with respect to Fc|Fc$^+$ as will be described in section 2.3.5.

A potentiostat controls the potential difference between the working and reference electrodes (referred to as the applied potential) thereby providing energy for an electrochemical reaction to occur at the WE surface. Adsorption and desorption can occur, and the structure of the surface of the electrode can change with potential or solution composition. External currents can flow when the potential, electrode area, or solution composition changes. In electrochemistry, there are two types of current measured at the electrode-solution interface - Faradaic current and non-Faradaic current. In a Faradaic process, electrons are transferred between an electrode and an analyte, usually causing oxidation or reduction of an ion or atom. Non-Faradaic current arises when charged particles do not cross the interface.[28] The current produced from the reaction at the WE is balanced by the counter electrode (CE). A current flowing in the opposite direction at the CE balances the WE and prevents excess current from reaching the reference electrode (RE).

To collect cyclic voltammograms, a molecule was dissolved in electrolyte solution and pipetted into the electrochemical cell. The ceramic containing all three electrodes was placed in the cell so that all the electrodes were submerged in solution. The cell was then connected to a circuit board and the potentiostat. The potentiostat is used to apply a potential, or energy, between the RE and the WE. When the potential was sufficient, current resulting from electron-transfer reactions at the WE surface were measured. The recorded cyclic voltammogram consists of the current response (measured in amps, A) as a function of applied potential (volts, V). A more detailed discussion of cyclic voltammetry follows in section 2.3.2.

Electrochemical reactions during electrochemical measurements occur in a mixture of solvent and supporting electrolyte, commonly termed the electrolyte solution. As electron transfers occur, charge neutrality is maintained by the migration of ions in the electrolyte solution. An electrolytic solution with good solvating power is needed to dissolve reactants and products, allow for rapid

transport of reactants and products to and from the electrodes, and mitigate side reactions that may occur with a reactive species created at electrodes.[29] Ideal solvents dissolve the analyte and high concentrations of supporting electrolyte completely, are stable in the potential range of the experiment, and do not lead to side reactions with the analyte or supporting electrolyte.[30] The supporting electrolyte is a salt dissolved in the chosen solvent that decreases solution resistance by increasing solution conductivity. Generally, strong electrolytes (electrolytes that fully dissociate into ions when dissolved) are chosen for electrochemical experiments. As electron transfers occurs at the electrodes, the supporting electrolytes diffuses to balance the charge. The increase in conductivity eliminates analyte migration in the electric field (positive ions moving to negative electrodes). Eliminating analyte migration in the electric field increases the probability that the electrolyte will migrate to the electrode interface minimizing impacts of solution resistance.

Even at high salt concentrations, electrolyte solutions have an intrinsic resistance (the tendency to stop the flow of current). Some potentiostats can compensate for solution resistance but a small amount of uncompensated resistance between the working electrode and reference electrode remains. This uncompensated resistance impacts the measured potential during experiments such that the potential needed for an electron transfer reaction to occur may not be proportional to the applied potential, decreasing the accuracy of the measurement. The potential needed to overcome solution resistance is called ohmic drop and is equal to the product of uncompensated resistance and current passed. Ohmic drop is minimized by decreasing the physical distance between the RE and the WE, and by increasing the conductivity of solution using supporting electrolytes. High concentration of supporting electrolyte ensures the potential difference applied to the cell is localized at the solution-electrode interface such that the measured potential is nearly proportional to the applied potential. Additionally, the impact of migration of analyte is negligible relative to that of diffusion (analyte moving from a region of high concentration

37

to a region of low concentration) and diffusion is linearized (diffusion comes from one direction).[30]

Working electrodes must be electrochemically inert over a wide potential range such that they do not generate current in response to an applied potential, degrade with use, nor chemically react with the analyte, solvent, and electrolyte species. Common WE materials for cyclic voltammetry are platinum, gold, mercury, and glassy carbon. Counter electrodes must be chemically and electrochemically inert and have a surface area equal to or larger than, that of the WE to balance the generated current at the WE. Generally, a CE with ten times the surface area of the WE (or more) is preferable. Common CE materials include platinum, gold, graphite, or glassy carbon. Reference electrodes must have a defined, stable, and reproducible equilibrium potential independent of the electrolyte used in the cell. Common materials include silver/silver chloride and the saturated calomel. [31]

### 2.3.1 Electron transfer reactions at the electrode surface

An ion or molecule is oxidized (or reduced) at the electrode-solution interface when the applied potential is sufficient.[29] For example, the analyte $O$ is converted to its reduced form $R$ when $n$ number of electrons are added to the ion (Equation 2.4).

$$O + ne^- \rightarrow R \qquad\qquad (2.4)$$

The potential energy that drives the redox processes can be determined from the applied potential, $E$. For a redox process with fast electron-transfer kinetics, the concentrations of the oxidized [O] and reduced [R] analyte are related to the applied potential, by the Nernst equation (Equation 2.5).

$$E = E^0 + \frac{RT}{F} ln \frac{[O]}{[R]} \qquad\qquad (2.5)$$

where $E^0$ is the standard reduction potential (V), $F$ is Faraday's constant (F = 96,485.3 C mol$^{-1}$), $R$ is the gas constant (8.3145 J mol$^{-1}$ K$^{-1)}$), $n$ is the number of electrons, and $T$ is temperature in Kelvin. Concentrations of redox-active species at the electrode interface change as electron transfer reactions occur until equilibrium as defined by the Nernst equation, is reached.

The standard reduction potential can be related to free energy change ($\Delta G^0$) and the equilibrium constant (K) as shown in Figure 2.7.



| $\Delta G^0$ | $E^0_{cell}$ | K | Direction of Reaction |
|---|---|---|---|
| < 0 | > 0 | > 1 | Spontaneous in forward direction |
| > 0 | < 0 | < 1 | Spontaneous in reverse direction |
| 0 | 0 | 1 | No net reaction; system at equilibrium |

**Figure 2.7** The relationships between $\Delta G^0$, K, and $E^0_{cell}$, each of which can be used to determine if an electron transfer reaction will occur spontaneously.
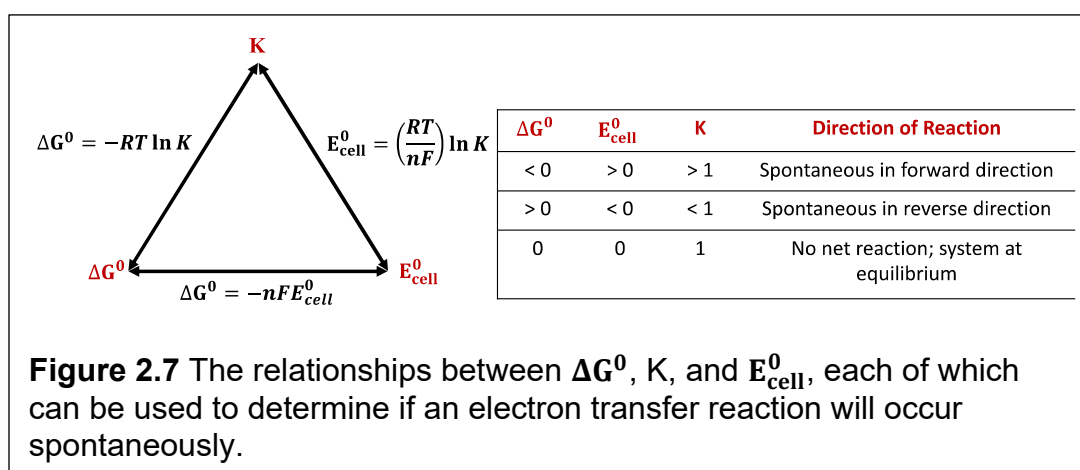
### 2.3.2 Theory of Cyclic Voltammetry

Cyclic voltammetry is an electrochemical technique where current is recorded as an applied potential is changed (swept) linearly between two values. The current response is recorded as a function of applied potential and the trace collected is a cyclic voltammogram. The applied potential (E) is represented on the x-axis and the current response (i) on the y-axis as shown in Figure 2.8a. An arrow is shown on a cyclic voltammogram to indicate the beginning and direction of the potential sweep, and the potential as a function of time is shown in Figure 2.8b. Typically, the caption of a cyclic voltammogram (cv) details other relevant parameters including analyte and electrolyte concentrations, scan rate, and the compositions of the electrodes.

**Figure 2.8** Cyclic voltammogram of 10 mM Fc at 100 mV/s (a.) and applied potential as a function of time for a generic cyclic voltammetry experiment (b.).
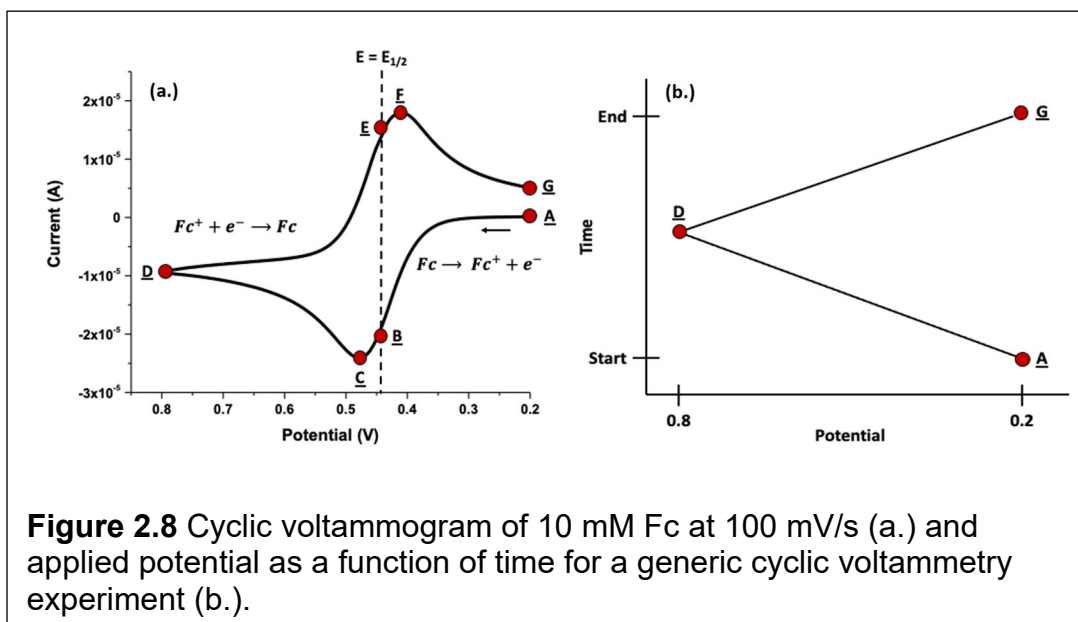
The trace in Fig 2.8b. shows the applied potential as a function of time with the x-axis corresponding to the cyclic voltammogram in Fig 2.8a.[30] The scan begins at an initial potential, **A**, is swept towards **D**, and then reversed and swept in the opposite direction to **G**. This forms one cycle of the cyclic voltammogram. The applied potential controls the driving force for any redox events the analyte might undergo. As the potential is applied, the current at the WE is measured, yielding a cyclic voltammogram.

At the molecular level, a cyclic voltammogram can be thought of as changes in concentration profiles of the redox-active species near the working electrode surface resulting from the potential sweep and planar diffusion.[29] The relative concentrations of analyte species change as the potential is swept when the analyte molecules nearest the electrode surface are oxidized (or reduced). For example, during an oxidation, a neutral species ($Fc$) is oxidized to a +1 oxidation state ($Fc^+$) (Equation 2.5).

$$Fc \rightarrow Fc^+ + e^- \qquad (2.5)$$
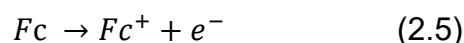
As the potential scanned from point **A** to point **D** in the voltammogram shown in Fig 8a., the more neutral molecules are oxidized, the concentration of the $Fc^+$

near the electrode increases, and the distance the neutral molecules travels (diffuses) to the working electrode increases. The observed increase in current is proportional to the number of analyte molecules that undergo oxidation. The current response increases until it reaches a maximum or peak current at point **C.** Peak current is discussed in detail in Section 2.3.4.

  When the potential sweep direction is reversed at point **D**, the oxidized analyte molecules (Fc⁺) nearest the electrode surface are reduced to neutral species (*Fc*) (Equation 2.6) from point **D** to point **G**.


$$Fc^+ + e^- \rightarrow Fc \qquad (2.6)$$
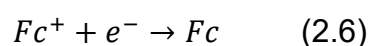

As more oxidized molecules are reduced, the concentration of the neutral molecule near the electrode increases, and the distance the oxidized molecule diffuses to the working electrode increases. Diffusion is discussed in detail in Section 2.3.3. The observed increase in current is proportional to the number of analyte molecules that undergo reduction. The current increases until it reaches a peak current **(F)**. The concentrations of *Fc* and *Fc⁺* are equal at the working electrode at points **B** and **E** and the dotted line corresponds to the $E_{1/2}$. $E_{1/2}$ values are discussed in detail in Section 2.3.4.

  The layers of charged species at the electrode-solution interface are shown in Figure 2.9.[29] and referred to as the electrical double layer.[32] The Helmholtz layer is the region closest to the electrode and is occupied by counterions (electrolyte ions with the charge opposite that of the electrode surface charge) that are specifically adsorbed (electrostatically) to the electrode surface. The Helmholtz layer is divided into two subregions – the inner Helmholtz (IHP) and outer Helmholtz (OHP) planes. The IHP is contains the specifically adsorbed ions. The OHP contains solvated ions closest to the electrode surface and consists of solvated ions interacting with the surface of the electrode through long-range electrostatic forces (nonspecifically adsorbed).[33] The diffuse layer is composed of nonspecifically adsorbed ions (or molecules) and extends from the

OHP to the bulk solution. Beyond the diffuse layer, electrostatic impacts initiated by the electrode surface do not affect ions (or molecules).



**Figure 2.9** The interfacial electrical double layer formed at the anode. Most solvent molecules were omitted for clarity.
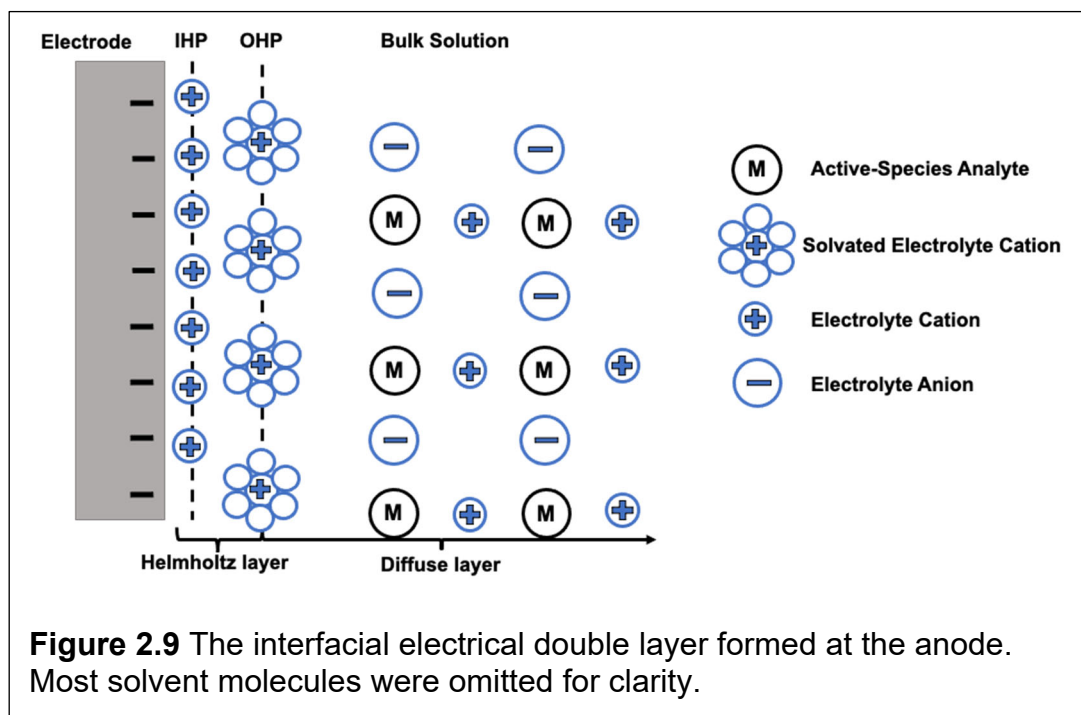
*2.3.3 Diffusion*

Diffusion is one mode of mass transfer that may determine the current at the electrode as a function of time and potential. Consider Equation (2.7):

$$O + ne^- \rightleftharpoons R \qquad (2.7)$$

Where O is the oxidized species, n is the number of electrons, and R is the reduced species. The set of equilibria involved in the diffusion of the reactant towards the electrode (**A**), the reaction at the electrode (**B**), and the diffusion of the product away from the electrode surface into the bulk solution (**C**) is shown in Figure 2.10.[29]

42

**Figure 2.10** Diffusion of a generic species showing diffusion to the electrode (<u>A</u>), electron transfer (<u>B</u>), and diffusion away from electrode (<u>C</u>) for reduction and oxidation reactions.
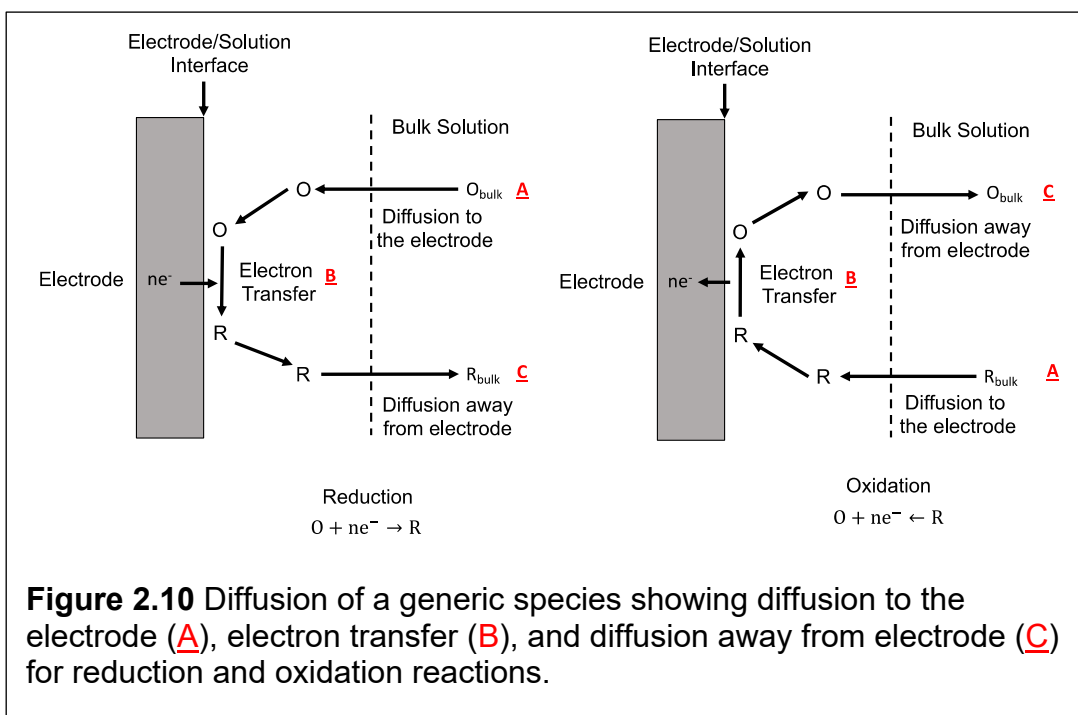
Anodic currents are produced by a species diffusing (i.e., moving against the concentration gradient) toward the anode until reaching the surface and undergoing an electron transfer reaction, and cathode currents by cations diffusing toward the cathode and undergoing an electron transfer reaction. When the reaction rate is equal to or faster than the rate of diffusion, the reaction is considered to be diffusion-limited.[29]

For this project, a large planar working electrode was used. Conventional electrode diffusion comes from one direction or the electrode surface (i.e., linear, or planar). The redox active molecules close to the electrode/solution interface are depleted and current decays with time shown by the Randles-Sevcik equation (Equation 2.8):

$$i_p = 0.4463 \, nFAC \left(\frac{nFvD}{RT}\right)^{1/2} \qquad (2.8)$$

where $i$ (A) is the current, $n$ is the number of electrons transferred between O and R, $F$ is Faraday's constant (1F = 96,485.3 C mol$^{-1}$), $A$ (cm$^2$) is the electrode area, $D$ (cm$^2$ sec$^{-1}$) is the diffusion coefficient for the species O, $v$ (mV/s) is the scan rate R is the gas constant (8.3145 J mol$^{-1}$ K$^{-1}$), and T (K) is temperature. Assuming linear diffusion is the only contributor of overall current, this equation helps to determine the current as a function of time or the time that a molecule of O takes to diffuse a certain distance. For this project, the diffusion coefficient was calculated from a plot of $i$ vs. $v^{-1/2}$. Using the slope of the line, $D$ was found using Equation (2.9):

$$D = \frac{(slope)^2 \pi}{(nFAC^*)^2} \qquad\qquad (2.9)$$

Deviations from linearity suggests electrochemical quasi-reversibility or electron transfer reactions occurring by electrode surface-adsorbed species. If the reaction is quasi-reversible, the diffusion coefficient can be determined through an alternative route (e.g., rotating disk electrode).

### 2.3.4 Characterization using cyclic voltammetry

 Cyclic voltammetry offers rapid screening of redox properties of electroactive species including but not limited to the thermodynamics heterogeneous electron transfer reactions (or redox processes), the chemical reversibility of the processes, and the electrochemical reversibility, a measure of electron transfer kinetics. Thermodynamics – how much energy is required to oxidize or reduce a molecule – can be measured by monitoring peak positions and shapes. Electron transfer thermodynamics can be determined by comparing $E_{1/2}$ values.[34] Reaction kinetics – how fast electron transfer occurs – can be determined by measuring peak potentials and peak currents as a function of scan rate.

Electrochemical reversibility describes the rate of electron transfer between the working electrode and bulk solution.[32] Electrochemically reversible reactions are characterized by high electron transfer rates ($k^0 > 10^{-1}$ cm s$^{-1}$) at the electrode/solution interface. The measured current is limited only by diffusion of the redox active molecules to the working electrode, where the peak potentials and peak separation are independent of the scan rate. Electrochemically reversible reactions yield the "duck curve", with forward and reverse peaks of similar magnitude.

Electrochemically irreversible reactions are characterized by slow electron transfer rates ($k^0 < 10^{-5}$ cm s$^{-1}$). The measured current is limited by slow charge-transfer kinetics; extreme electrode potentials are required to drive the electron transfer. Peak potentials shift more negative for reduction and more positive for oxidation with increasing scan rates leading to increased peak separation. Irreversible reactions yield forward and reverse peaks of different magnitude. Quasi-reversible electrochemical reactions have intermediate electron transfer rates between reversible and irreversible ($k^0$ falls between $10^{-1}$ and $10^{-5}$). The measured current is limited by both charge-transfer kinetics and diffusion. Quasi-reversible processes are characterized by scan rate-dependent peak potentials. Peak separations values and peak shapes are between those of reversible and irreversible systems. The range of electron transfer rates from reversible, quasi-reversible, to irreversible is one continuum.[35]

Peak potentials are the potentials at which the current reaches a maximum (or minimum). The two peaks are distinguished by referring to the peak corresponding to oxidation, anodic, and the peak corresponding to reduction, cathodic. The anodic peak appears as the analyte is oxidized at the anode and the cathodic peak as the analyte is reduced at the cathode. The difference between the anodic and cathodic peak potentials – peak separation – is a result of the diffusion of analyte to and away from the working electrode. This parameter can be used to determine electrochemical reversibility.

Electrochemically reversible voltammograms are characterized by peak separations of 57/n mV where n is the number of electrons transferred. The

peak values remain constant at varying scan rates. Potentials shifting to more extreme values (more negative for reduction; more positive for oxidation) as scan rate increases is characteristic of electrochemical irreversibility. Peak separations are greater than 200/n mV. Quasi-reversible separations are between those of reversible and irreversible systems and increase with scan rate.

Integration of the area under the curve corresponding to oxidation (or reduction) yields the peak charge, which is proportional to the number of molecules undergoing electron-transfer reactions. If the product is stable on the time scale of the experiment and the reaction is chemically reversible, the peak current observed for the return scan should be equal to that seen for the forward scan as shown in Equation (2.10).

$$\frac{i_{ox}}{i_{red}} = 1 \qquad (2.10)$$

Peak currents will increase linearly as a function of the square root of the scan rate for reversible electron transfers. Plots of $i_p$ vs $\sqrt{v}$ are useful in the characterization of electrochemically reversible redox systems. Deviations from linearity are indicative of either complication in the kinetics of the electron transfer or the result of chemical changes that occur because of electron transfer (homogenous reactions).

In cyclic voltammetry, $E_{1/2}$ is the midpoint between the anodic and cathodic peak potentials. To determine the value of $E_{1/2}$, the anodic and cathodic peak potentials corresponding to a forward and reverse electron transfer event are identified as points A and B, respectively, and averaged (Equation 2.11).

$$E_{\frac{1}{2}} = \frac{A+B}{2} \qquad (2.11)$$

The $E_{1/2}$ value can be used to estimate the redox potential of the reaction – the energy needed for the electron transfer reaction to occur. The redox potential of

a given species can be tuned by adding electron-donating (or electron-withdrawing) substituents to the molecule. In a redox flow battery, two redox active molecules are used in the separate electrolyte tanks and corresponding half-cells. The difference between the redox potentials of the two species determines the voltage, so tuning the redox potential of each species using substituents is employed to maximize the cell voltage.

### 2.3.5 Ferrocene as an internal reference

Although an Ag|AgCl reference electrode was used for data collection, the potential of the electrode can vary between experiments due to variations in [$Ag^+$], electrolyte, or solvent used.[30] Alternatively, potentials are referenced to ferrocene (Fc), a common internal reference compound. As a shown in Figure 11, the potential axis for **1** referenced to Ag|AgCl (Fig 2.11a.) is converted to Fc/Fc$^+$ shown in Fig 2.11b. A cyclic voltammogram of 10 mM Fc (DCM, 0.50 TBABF$_4$) is collected using the electrodes and electrochemical cell that will be used to characterize the analyte. The $E_{1/2}$ value was calculated to be +0.444 V vs. Ag|AgCl, and this value is considered 0.000 V vs. Fc|Fc$^+$. After the cv's of the analytes are collected, the potential axis is converted from a reference of Ag|AgCl to a reference of Fc|Fc$^+$. In this example, the $E_{1/2}$ of **1** is +0.588 vs. Ag|AgCl and +0.106 V vs. ferrocene.
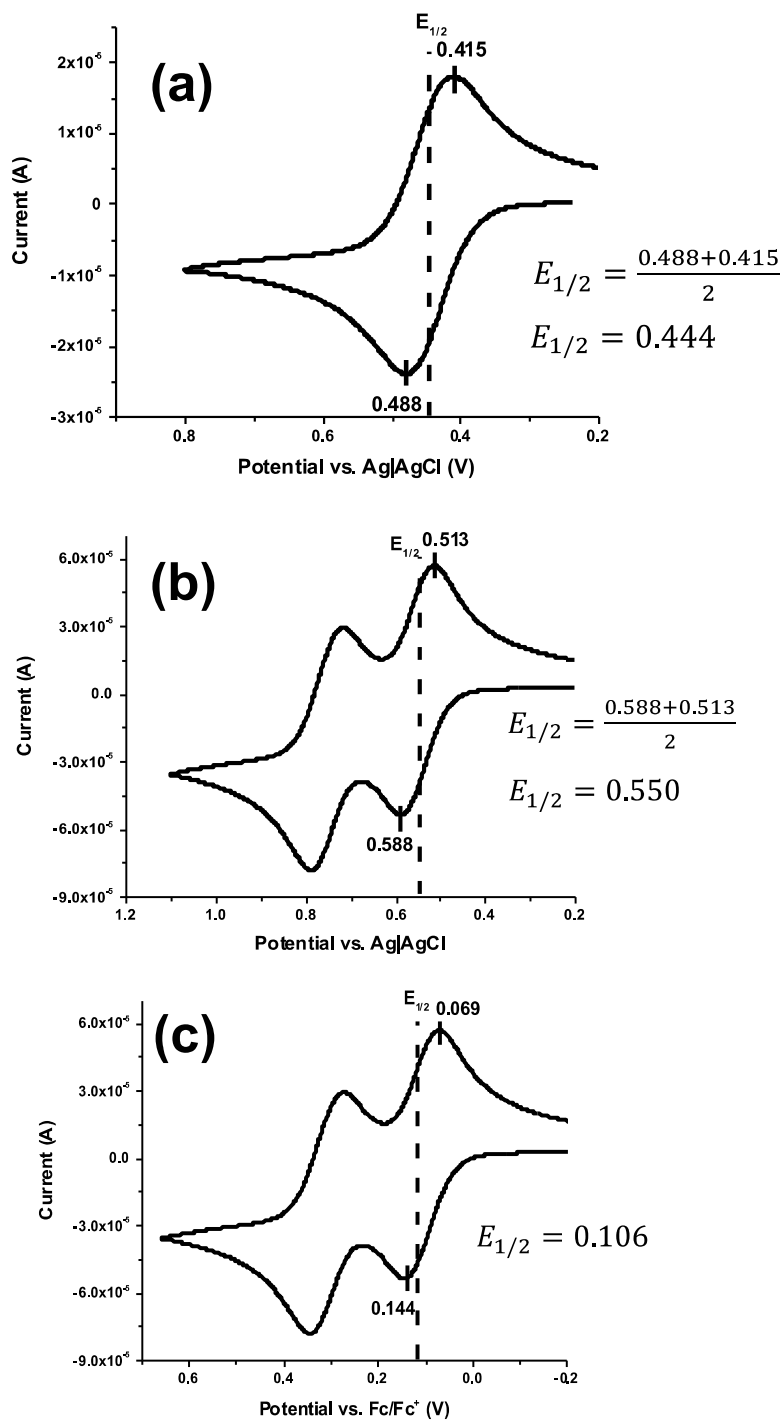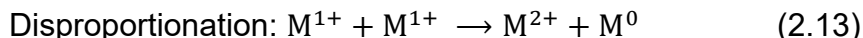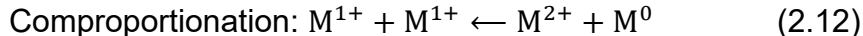
**Figure 2.11** Cyclic voltammograms of 10 mM Fc (DCM, 0.50 M TBABF4) (a.), and 10 mM Molecule (1) (DCM, 0.50 M TBABF4) referenced to Ag|AgCl (b.) and referenced to ferrocene (c.) at 100 mV/s. Notice the E1/2 for ferrocene (0.444 V) is set to zero after potentials are converted.

## 2.3.6 Mixed valence systems

In this project, we are working with molecules that can undergo two electron transfer reactions and therefore exist in three oxidation states -- neutral, +1 (cation), and +2 (dication) – referred to as mixed-valence species. In the cyclic voltammogram of a mixed-valence species, the resolution of the two redox events reflects the equilibrium positions of the species when all three oxidation states are present in the same solution.   The oxidation states can react with each other by comproportionation and disproportionation. Comproportionation (Equation 2.12) occurs when two reactants of the same molecule but different oxidation states, form a product in which the molecules reach the same oxidation number. Disproportionation is the opposite of comproportionation, two reactants of the same molecule and the same oxidation states form a product where the molecules have different oxidation states (Equation 2.13.).[32]

$$\text{Comproportionation: } M^{1+} + M^{1+} \longleftarrow M^{2+} + M^0 \qquad (2.12)$$

$$\text{Disproportionation: } M^{1+} + M^{1+} \longrightarrow M^{2+} + M^0 \qquad (2.13)$$

The difference in the two $E_{1/2}$ values (Figure. 2.12). can be used to determine the disproportionation constant ($K_{disp}$) as shown in equation (Equations 2.14 and 2.15). If $K_{disp}$ is small, the reaction lies to the left and the molecule is expected to stay in the +1 state in the presence of $M^0$ and/or $M^{2+}$.[32] The meaning of $K_{disp}$ will be discussed in Chapter 3.

$$K_{disp} = \frac{k_f}{k_b} = \frac{[M^{2+}][M^0]}{[M^{+1}]^2} \qquad (2.14)$$

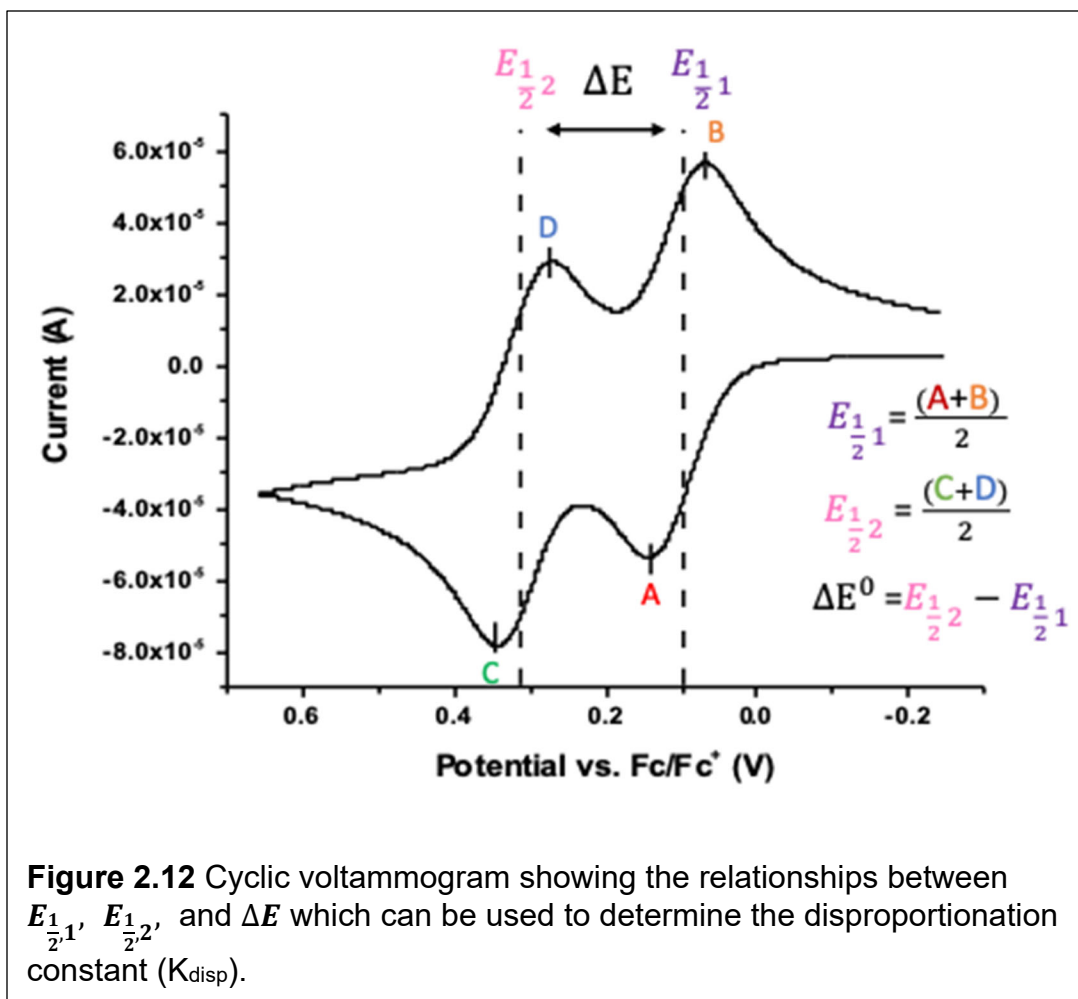$$K_{disp} = e^{[\frac{(\Delta E^0)(F)}{RT}]} \qquad (2.15$$

**Figure 2.12** Cyclic voltammogram showing the relationships between $E_{\frac{1}{2},1}$, $E_{\frac{1}{2},2}$, and $\Delta E$ which can be used to determine the disproportionation constant ($K_{disp}$).

The disproportionation constant is used to evaluate mixed-valent compounds using the Robin-Day classification scheme which divides the molecules into three classes (Class I, Class II, Class III. Class I molecules have minimal to no (measurable) electronic communication and $K_{disp} < 10^2$. When a redox event occurs, the charge is localized on one redox center and the second redox event is not impacted by the first. The two electron transfer processes cannot be resolved which is observed in a cyclic voltammogram where $\Delta E^0$ is small (two poorly spaced waves or one wave).

Class III molecules have strong electronic communication; the charge is completely delocalized between both redox centers and $K_{disp} < 10^6$. When a redox event occurs, the second redox center can feel the presence of the loss (or gain) of an electron. To overcome the electronic communication and carry

out a second redox event the potential applied to the molecule and difference in potential between the two redox events are relatively large. The two electron transfer processes are well-spaced and $\Delta E^0$ is large.

Class II molecules have an intermediate degree of delocalization; the charge rests on the two side chains but there is some electronic communication. The K$_{disp}$ and spacing of redox events are between those of Class I and Class III. Figure 2.13 shows shapes of cyclic voltammograms as the value of $\Delta E^0$ increases.



**Figure 2.13** Shapes of cyclic voltammograms change at different values of $\Delta E^0$. (Figure taken from Bard et al.) [32]
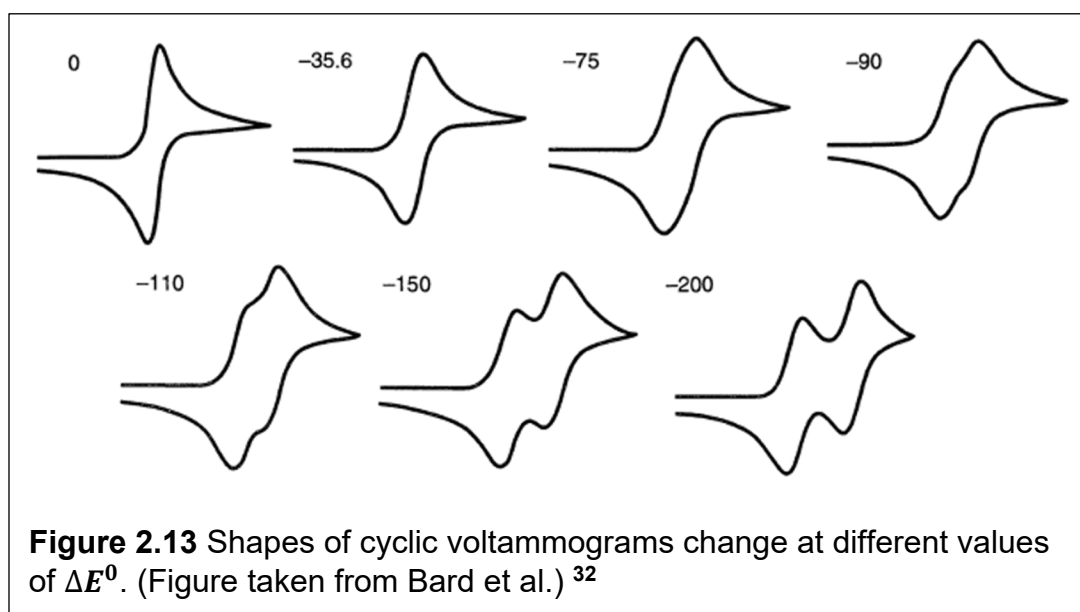
## 2.4 Spectroelectrochemistry

Electrochemistry provides information on the redox events occurring including the reactivity and stability of the molecule. However, electrochemistry lacks specificity. To better understand the electronic structure of the molecule as a function of oxidation sate, we investigate optical properties as a function of potential using spectroelectrochemistry. Spectroelectrochemical experiments relate the current measured during electrochemical oxidation (or reduction) to

changes in the electronic structure of the molecule. Spectroscopic signatures of the molecule at each applied potential are collected as each potential is held. The spectroscopic characterization of the molecule demonstrates the conversion from the neutral to +1 and +1 to +2 oxidation states.

Spectroelectrochemical measurements were completed using an Agilent 8454 diode array instrument and a CHI 440b potentiostat and a Pine spectroelectrochemical cell with a ceramic screen-printed multielectrode configuration and an external reference electrode (Au WE, Au CE, Ag|AgCl RE) as shown in Figure 2.14.



**Figure 2.14** Pine ceramic screen-printed electrode (A.), ceramic electrode in the cuvette (B. & C.), and the spectroelectrochemical cell connected to the circuit board and the potentiostat (D.).
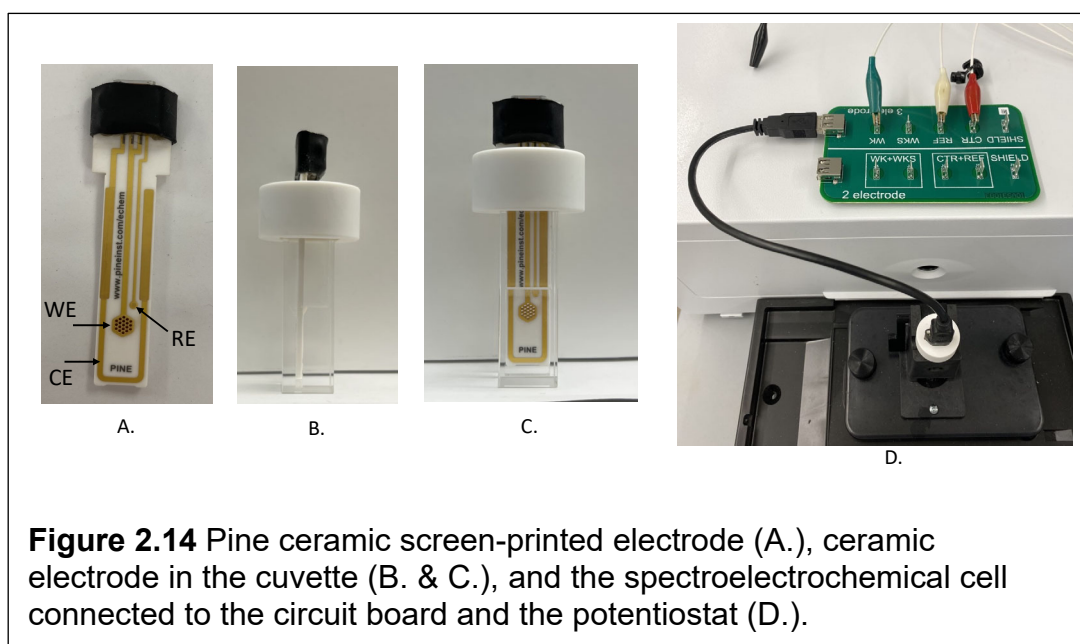
To collect spectroelectrochemical data, a blank was collected with electrolyte only. With no applied potential, an initial absorbance spectrum was collected for the neutral molecule. Next, a potential was applied for 60 seconds, at which point an absorbance spectrum was collected (potential still applied). This process was repeated in 20-60 mV increments in the potential range of the oxidation reaction. A representative collection of spectra collected in a spectroelectrochemical experiment are shown in Figure 2.15. A cyclic voltammogram for the same molecule is inset.

**Figure 2.15** Absorbance spectra of 0.1 mM Molecule (1) (0.1 M TBABF$_4$, DCM) with no applied potential (neutral, left) and as a function of potential (right) in the pine spectroelectrochemical cell (Au WE, Au CE, Ag|AgCl RE).
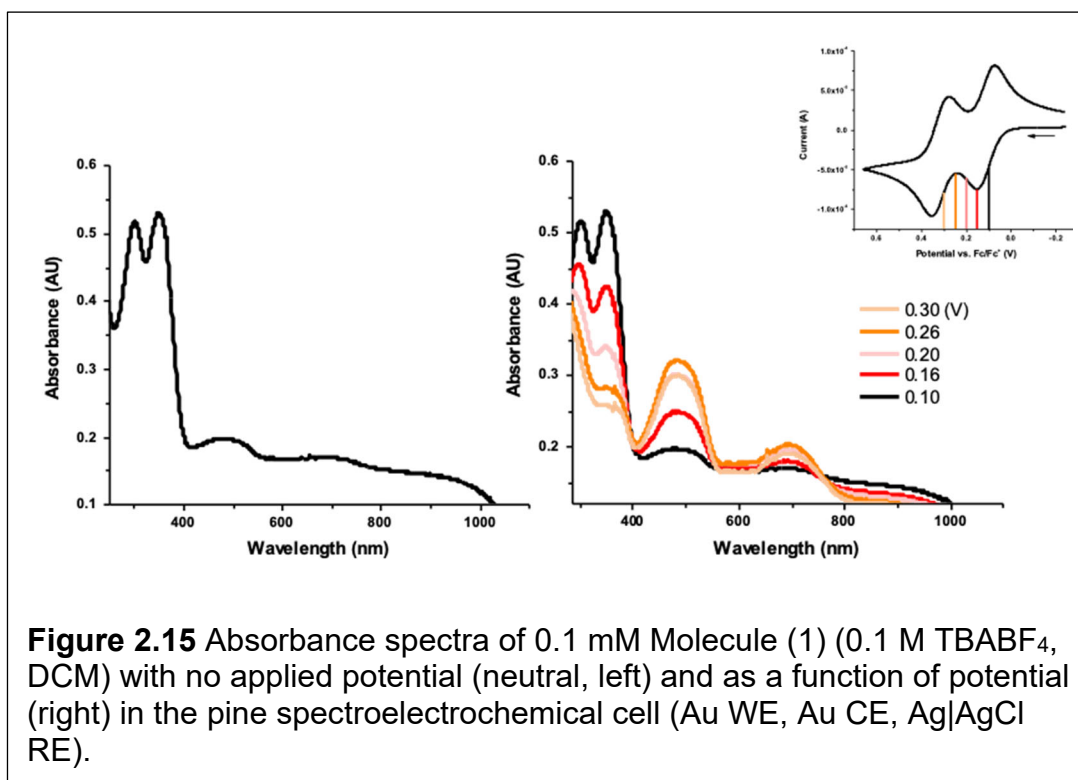
## 2.5 Computational Analysis

For this project all computations were provided by Rebekah Duke at the University of Kentucky and used a hybrid density functional theory (DFT) with long-range corrected functional (LC-wHPBE[1]) and a double zeta basis set (Def2SVP).

DFT is a quantum-mechanical method used to investigate electronic structures and properties of atoms, molecules, and solids. In DFT calculations, the molecular geometry, basis set used to determine the wavefunction, the properties to be calculated, and type(s) of calculations and assumptions are selected for input. Basis sets are used as approximate representations of atomic orbitals which are then used to calculate molecular orbitals using a linear

combination of atomic orbitals approximation. For this project, DFT was used to explore ground state and excited state structures and charge distributions.

## Chapter 3 Characterization of Molecules (1), (2) and (3)

The overarching goal of this work is to measure structure-property relationships in redox-active molecules for applications in redox flow batteries. The three molecules investigated are shown in Figure 3.1; each of these molecules is expected to undergo two electron-transfer events. The structural variations include the number of phenyl rings in the bridge between the two amino groups and the peripheral substituents. Changes in the bridge are expected to impact electronic communication between the two redox centers – the amino groups. The relative electron-withdrawing nature of the methoxy and trifluoro functional groups are expected to impact the amount of energy required for oxidation. Characterization of these species includes cyclic voltammetry to determine electrochemical reversibility, oxidation potentials, and disproportionation constants (Section 3.1), spectroelectrochemistry to determine the optical signatures of the neutral, cationic, and dicationic species (Section 3.2), spectral analysis of the redox-active species in the presence of a chemical oxidant to assess the stability of these species (Section 3.3), and computational modeling of the species to better understand the impacts of oxidation on shape and charge distribution (Section 3.4).

**Figure 3.1** Chemical structures of Molecules (**1**), (**2**), and (**3**) showing the bridge and peripheral substituents.
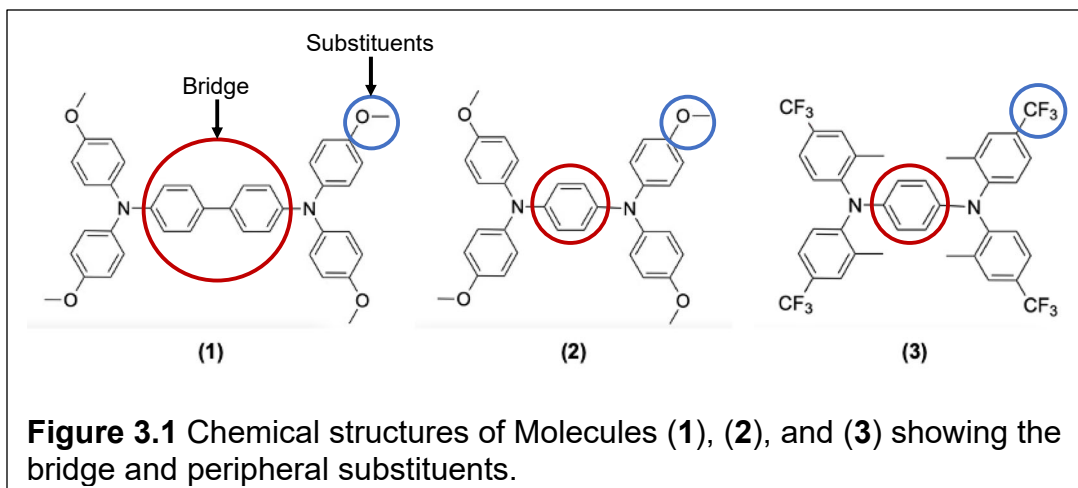
## 3.1 Cyclic Voltammetry

The initial step of the project was to monitor redox properties as a function of scan rate in solution and outside of a glovebox. Solutions of 1, 2, and 3 in dichloromethane (DCM) with tetrabutylammonium tetrafluoroborate (TBABF$_4$) or tetrabutylammonium hexafluorophosphate (TBAPF$_6$) were prepared and cyclic voltammograms were collected as shown in Figure 3.2. The molecules were only slightly soluble in acetonitrile which is a viable solvent for electrochemical measurements and more practical in battery applications due to low toxicity. The molecules are also soluble in dichlorobenzene, but this solvent absorbs in the ultraviolet region of the electromagnetic region and masks the presence of the cationic optical features of the three molecules. For this project, the same solvent (DCM) was used for all experiments to reduce variability in solvent-molecule interactions. Cyclic voltammograms were collected in a Pine electrochemical cell with a ceramic 3-electrode configuration. Though an Ag|AgCl RE was used for data collection, cyclic voltammograms of ferrocene (Fc) were collected, and all potentials are reported here with respect to Fc|Fc$^+$. See Section 2.3.5 for a detailed discussion of this conversion.
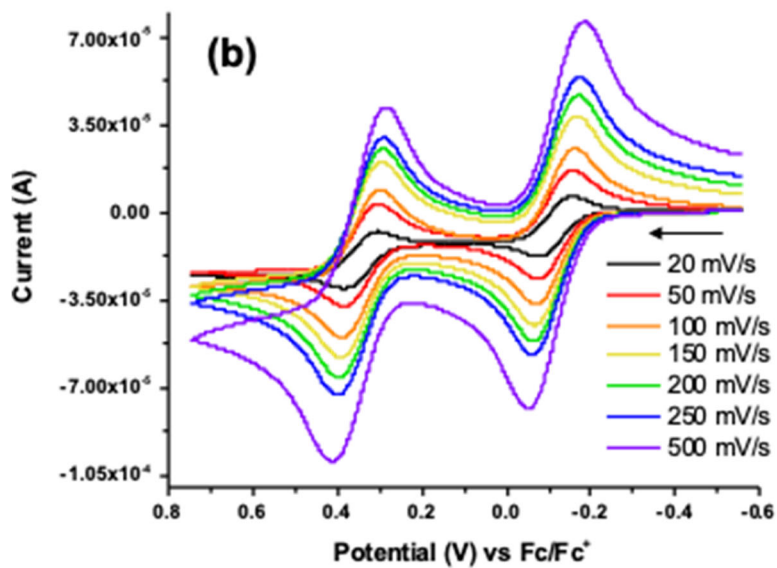
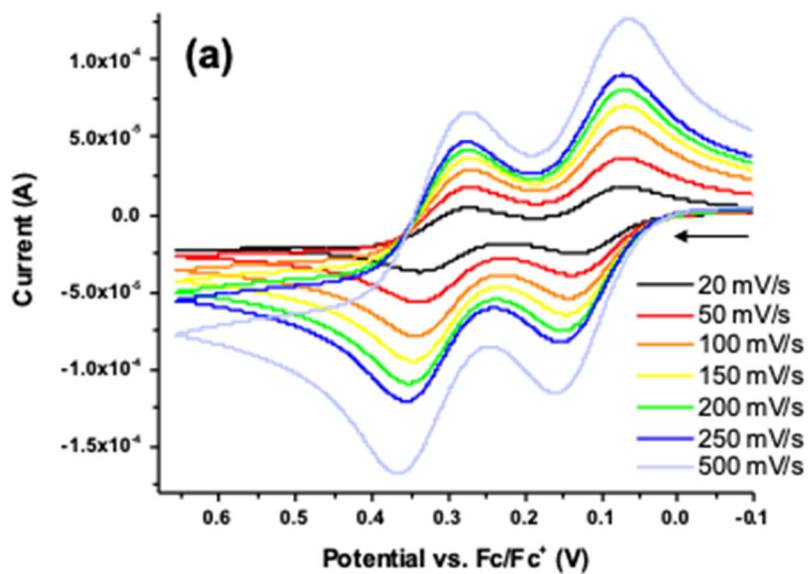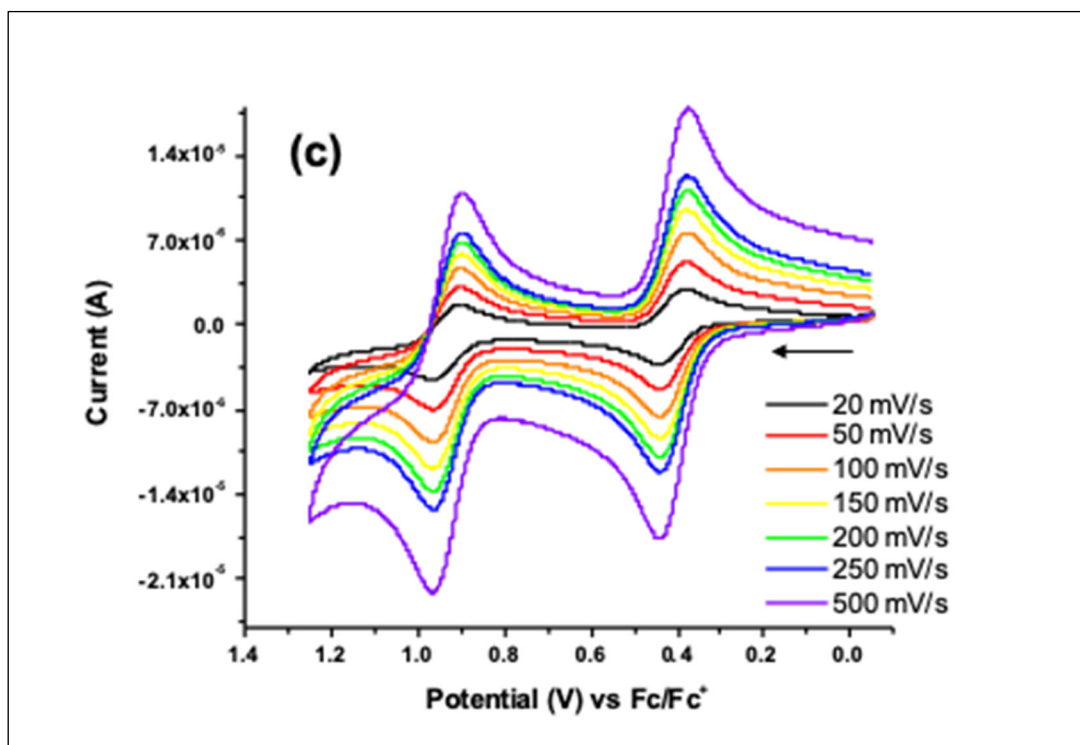**Figure 3.2** Cyclic voltammograms of 10 mM (**1**) (0.5 M TBABF$_4$/DCM) (a.), 0.1 mM (**2**) (0.1 M TBABF$_4$/DCM) (b.), and 1.0 mM (**3**) (0.25 M TBAPF$_6$/DCM) (c.) at varying scan rates. CVs were collected using a Pine electrochemical cell (Au WE, Au CE, Ag|AgCl RE) and referenced to Fc.

**Figure 3.2 continued**



As the potential was swept positively (100 mV/s), two discreet oxidation events were observed for all molecules; corresponding reduction events were observed when the potential was swept negatively. The general half reactions are shown in Equations 3.1 and 3.2.

$$M^0 \longrightarrow M^{+1} + e^- \qquad (3.1)$$

$$M^{+1} \longrightarrow M^{+2} + e^- \qquad (3.2)$$
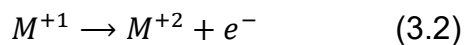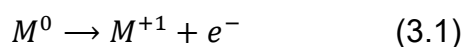
Using peak potential and peak separation values from cyclic voltammograms (Figure 3.3), ΔE and disproportionation constants were calculated (Table 3.1).

**Table 3.1** $E_{1/2}$, $\Delta$E, and Disproportionation values for molecules (**1**), (**2**), and (**3**).

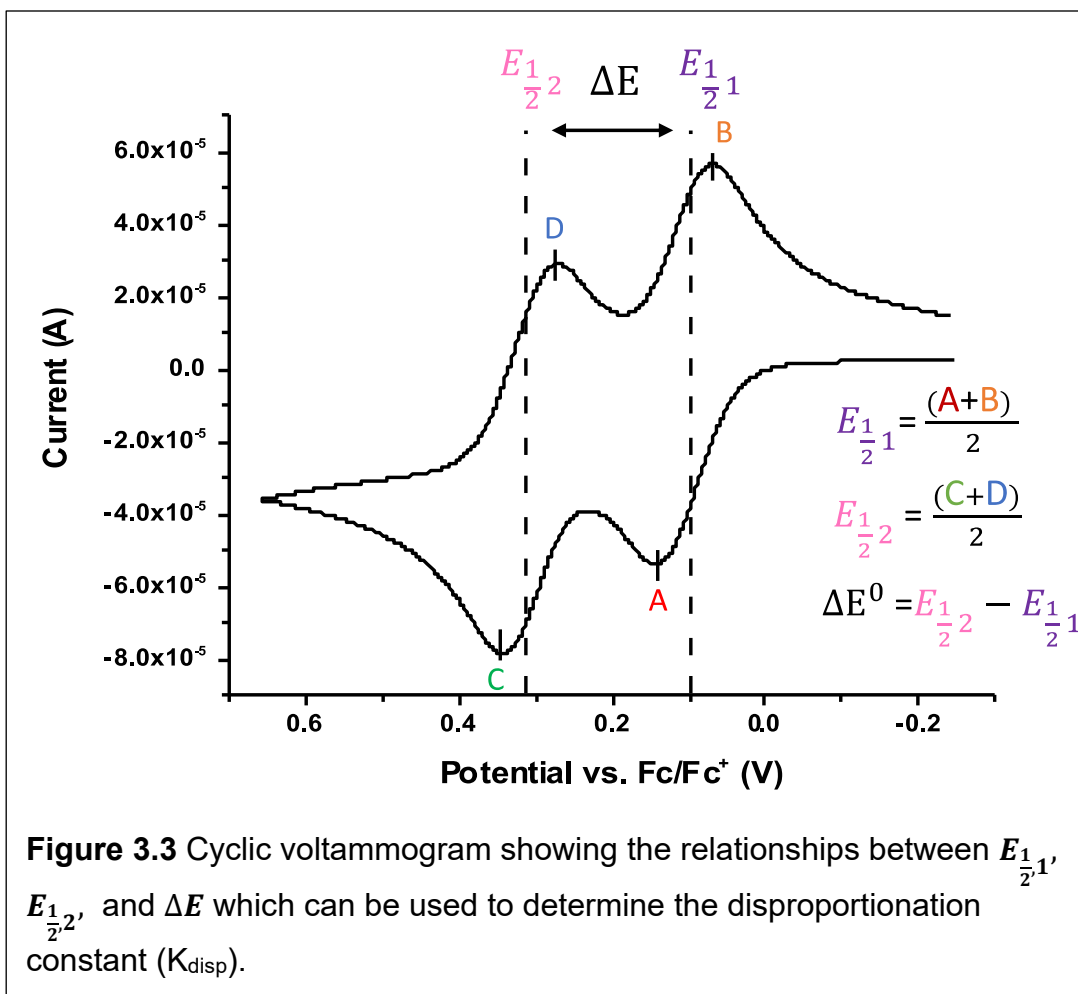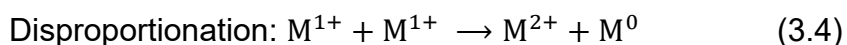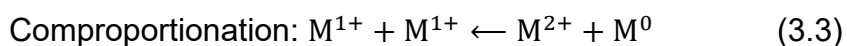| Molecule | $E_{\frac{1}{2}1}$ | $E_{\frac{1}{2}2}$ | $\Delta$E (V) | Disproportionation Constant, $K_{disp}$ |
|---|---|---|---|---|
| (**1**) | 0.105 | 0.307 | 0.201 | $3.70 \times 10^{-4}$ |
| (**2**) | -0.116 | 0.345 | 0.461 | $1.30 \times 10^{-8}$ |
| (**3**) | 0.410 | 0.933 | 0.523 | $1.10 \times 10^{-9}$ |



**Figure 3.3** Cyclic voltammogram showing the relationships between $E_{\frac{1}{2},1}$, $E_{\frac{1}{2},2}$, and $\Delta E$ which can be used to determine the disproportionation constant ($K_{disp}$).

The difference between the anodic and cathodic peak potentials – peak separation, $E_{1/2}$ – for one redox event can be used to determine electrochemical reversibility. Peak separations for all molecules are greater than 200 mV and increase with scan rate, indicative of quasi-reversible redox processes.[32]

The difference in the two $E_{1/2}$ values reflects the equilibrium positions of mixed-valence species when all three oxidation states are present. The oxidation states can react with each other by comproportionation (Equation 3.3) or disproportionation (Equation 3.4). Molecules used in RFBs could be stored in charged states for long periods of time. The disproportionation constant ($K_{disp}$) is used to determine the stability of the molecules in their charged states.[32]

$$\text{Comproportionation: } M^{1+} + M^{1+} \longleftarrow M^{2+} + M^0 \qquad (3.3)$$

$$\text{Disproportionation: } M^{1+} + M^{1+} \longrightarrow M^{2+} + M^0 \qquad (3.4)$$

For all trials completed, the $K_{disp}$ was determined to be small. When the neutral, singly oxidized, and doubly oxidized species are present comproportionation dominates. Based on this, we expect the molecules to stay in the singly oxidized state for relatively long periods of time.

The magnitude of $\Delta E$ for molecules undergoing two electron transfer events, that is to say the difference in potential for each of the two redox events, is indicative of the electronic structure of the molecule, described by the Robin-Day classification system, discussed in detail in Section 2.3.6. Briefly, if the electrons lost during oxidation are in discreet orbitals experiencing no electronic communication with one another (long, unconjugated bridge, for instance), little to no peak splitting is apparent in the voltammogram, and $\Delta E$ is expected to be near 36 mV. Conversely, if the electrons lost originate from the same orbital or orbitals with some electronic communication (short, conjugated bridge, for instance), clear peak splitting is expected, evidenced by a $\Delta E$ of greater than 125 mV.[32] Peak splitting values ($\Delta E$) can be tuned by changing the molecular

structure; large peak splitting values imply more extreme potentials are required to complete the second oxidation (due to the addition of an electron withdrawing group, for instance). That is to say, the second oxidation will require more energy than the first because the electronic environment of the second electron is electron-deficient relative to that of the first electron lost to oxidation.[36] For all three molecules analyzed in this work, clear peak splitting is observed, indicating some level of electronic communication between the redox centers.

Trends in ΔE can be attributed to differences in the peripheral substituents and/or the bridge lengths and conjugation of the molecules.[37] The conjugation length of **(2)** and **(3)** is small relative to **(1)**, and as expected, ΔE is larger for **(2)** and **(3)** relative to **(1)**. Molecules **(2)** and **(3)** experience the loss of the first electron more strongly than **(1)**; more positive potentials are required to complete the second oxidations. Molecule **(3)** has the largest peak separation suggesting the second oxidation requires more energy to complete relative to the same oxidation in **(1)** and **(2)** which was expected due to the addition of more electron-withdrawing substituents. Cyclic voltammograms showing the difference in potential ranges and peak separations are shown in Figure 3.4.

Other derivatives of bis-triaryl amines are expected to exhibit similar electronic properties. For example, a derivative with the bridge length of **(1)** and methoxy group substituted with -$CF_3$ at the para-positions would be expected to exhibit high oxidation potentials relative to **(1)** and **(2)** due to the highly electronegative character of the substituent. The peak splitting of such a derivative is expected to be small relative to **(2)** and **(3)** due to the longer conjugation of the molecule. The derivative would experience the loss of the first electron less strongly than **(2)** and **(3)**; less positive potentials are required to complete the second oxidation.
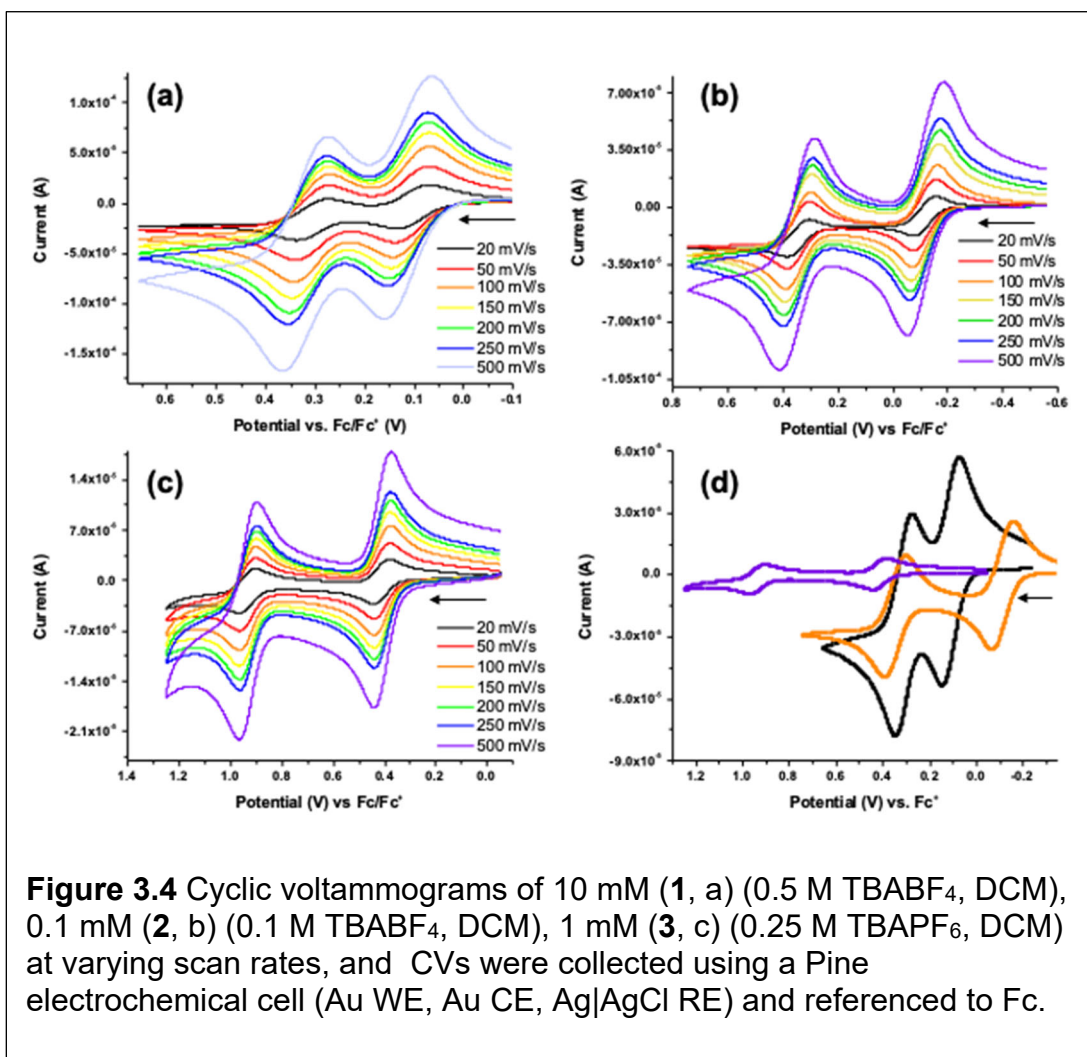
**Figure 3.4** Cyclic voltammograms of 10 mM (**1**, a) (0.5 M TBABF₄, DCM), 0.1 mM (**2**, b) (0.1 M TBABF₄, DCM), 1 mM (**3**, c) (0.25 M TBAPF₆, DCM) at varying scan rates, and  CVs were collected using a Pine electrochemical cell (Au WE, Au CE, Ag|AgCl RE) and referenced to Fc.

## 3.2 Spectroelectrochemistry

  Spectroelectrochemical experiments were used to correlate the electrochemical signals observed in voltammograms to optical changes. As shown in Figure 3.5, spectra of 0.1 mM solutions of all molecules as a function of potential were collected using a Pine spectroelectrochemical cell (Au WE, Au CE, Ag|AgCl RE) and referenced to Fc as described above. The spectral blank was collected with solvent and the electrodes present.

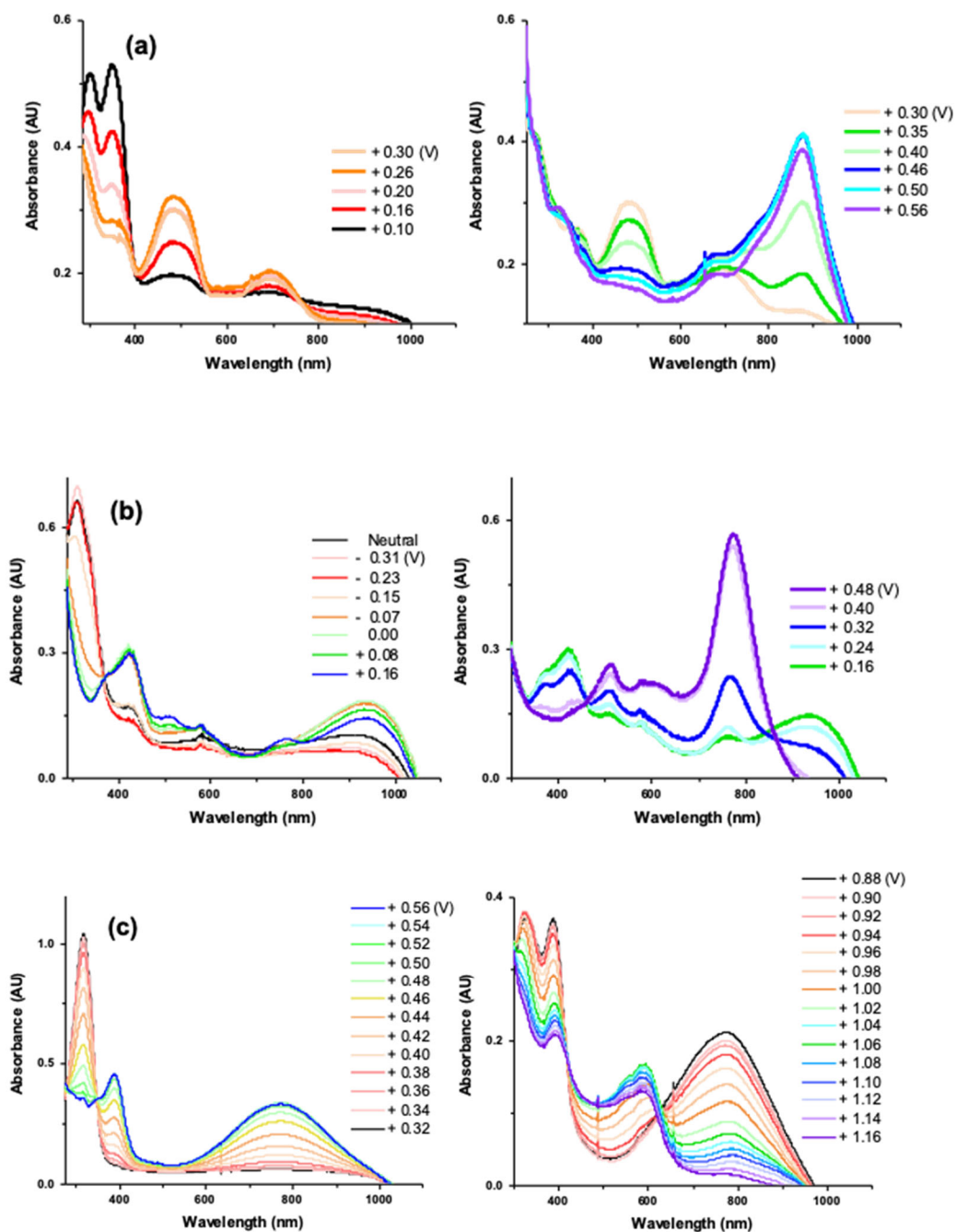**Figure 3.5** Absorbance spectra of 0.1 mM Molecules (**1,** a), (**2,** b) (0.1 M TBABF$_4$, DCM) and 0.1 mM Molecule (**3**, c) (0.25 M TBABF$_6$, DCM) as a function of potential in the Pine spectroelectrochemical cell (Au WE, Au CE, Ag|AgCl RE).

As the potential was stepped positively, absorbances near 350 nm for all molecules decreased in magnitude and absorbances near 486 nm **(1)**, 420 nm, 520 nm, and 950 nm **(2)**, and 395 nm and, 790 nm **(3)** were observed. Because the first oxidation events measured begin near the potentials at which the optical changes were observed, we attributed these spectral changes to the formation of singly oxidized species. When the applied potential was stepped to more positive potentials, the features of the singly oxidized species decreased in magnitude and absorbances near 698 nm and 876 nm **(1)**, 500 nm and 770 nm **(2)**, and 590 nm **(3)** were observed and generally increased in magnitude. The second oxidation event measured begins near the potentials at which these additional optical changes were observed, and we attributed these spectral changes to the formation of doubly oxidized species. Spectra corresponding to potentials between 0.56 V and 0.88 V of **(3)** were omitted. Because the second oxidation is separated by a relatively large magnitude, no redox activity or spectral changes are observed in this potential range. Figure 3.6 shows the spectra of the neutral, cationic, and dicationic species of all three molecules.
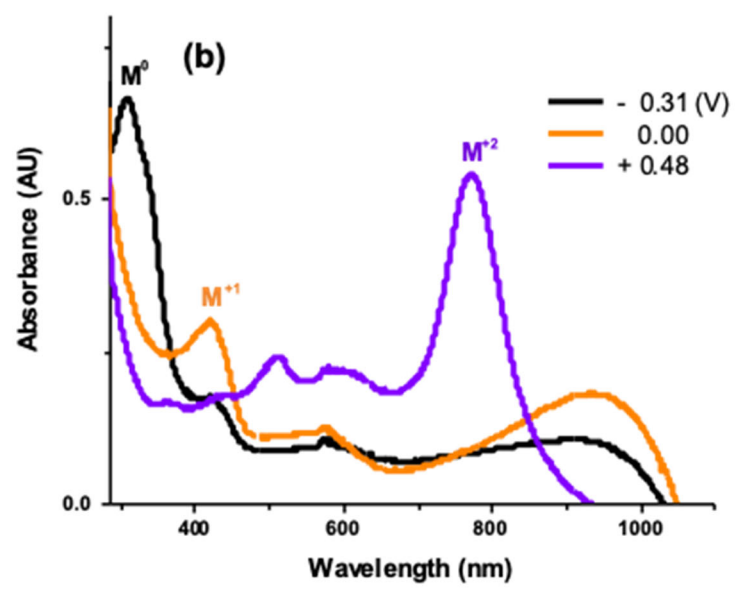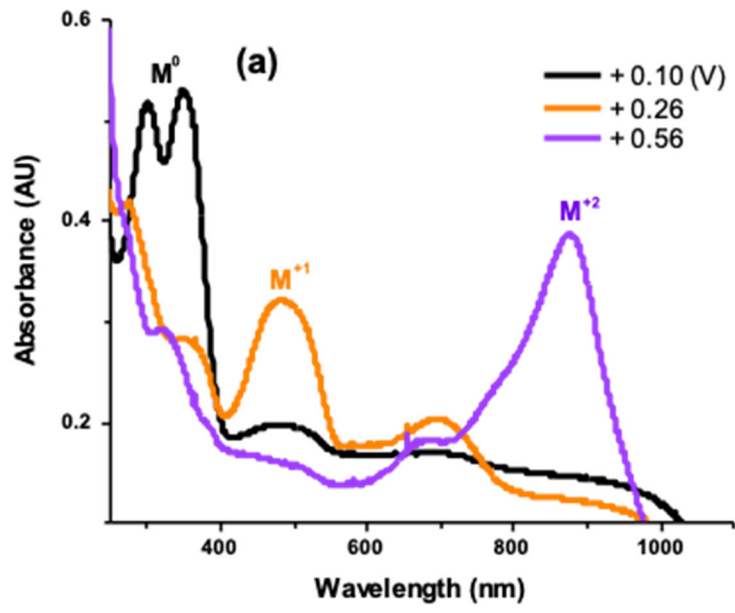
**Figure 3.6** Neutral, singly oxidized, and doubly oxidized spectral signatures for (**1**) (a), (**2**) (b), and (**3**) (c).

**Figure 3.6 continued**
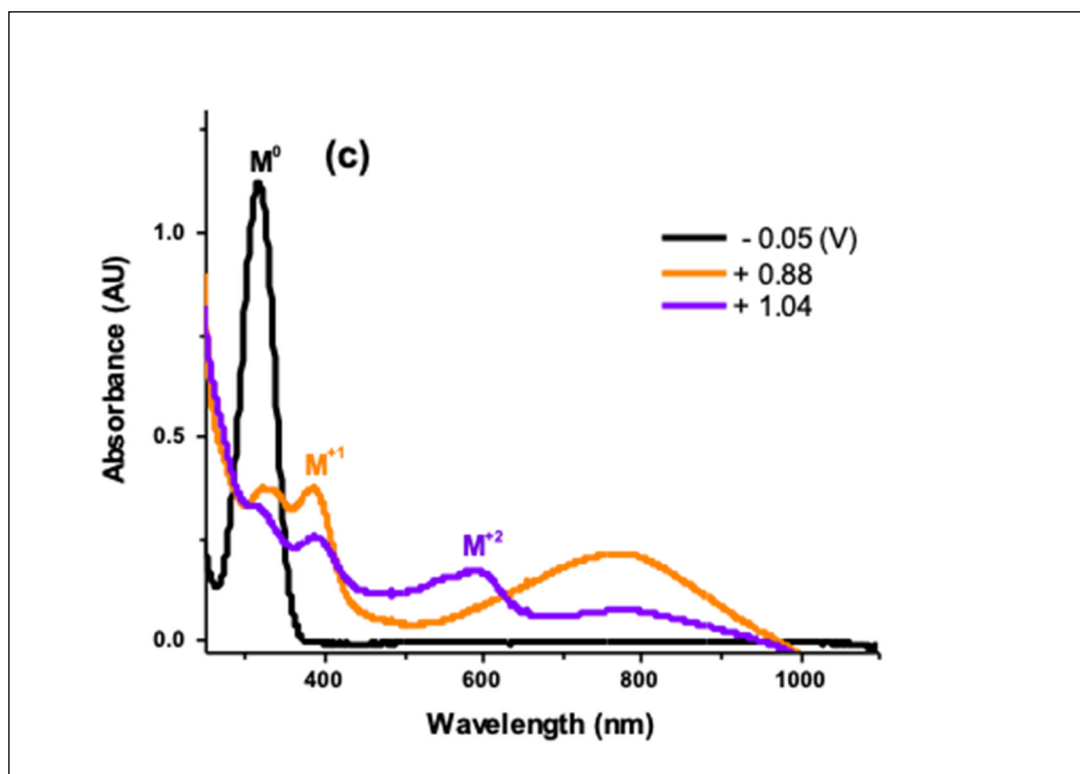


The spectral features of the cationic species, observed around 950 nm and 800 nm for **(2)** and **(3)**, respectively**,** are consistent with literature for mixed valence compounds.[38] Similar features for **(1)** may be observed in the near-infrared region, however the spectrophotometer used was limited to the ultraviolet-visible regions of the electromagnetic spectrum.

   As the cationic species is further oxidized to the dicationic species, the spectral features for the cationic species are not observed and features are observed around 890 nm and 780 nm for **(1)** and **(2)**, respectively. Similar features for **(3)** may be observed in the near-infrared region.

   Importantly, the neutral, cationic, and dicationic species of each molecule have distinct spectral features that can be monitored to determine the persistence of these species over time.

## 3.3 Chemical Oxidation

Chemical oxidants (magic blue and magic green) facilitate the transfer of electrons from species being oxidized (M) to the oxidizing reagent (X) as shown in Equations 3.3 and 3.4. Chemical oxidation can be used to support electrochemical oxidation data and determine the stability of the charged species over time. Absorbance spectra of magic blue and magic green are shown in Figure 3.7.

$$M^0 + X^+ \longrightarrow M^{+1} + X^0 \qquad (3.3)$$

$$M^{+1} + X^0 \longrightarrow M^{+2} + X^{-1} \qquad (3.4)$$



**Figure 3.7** Absorbance spectra of 0.05 mM Magic Blue (left) and Magic Green (right).
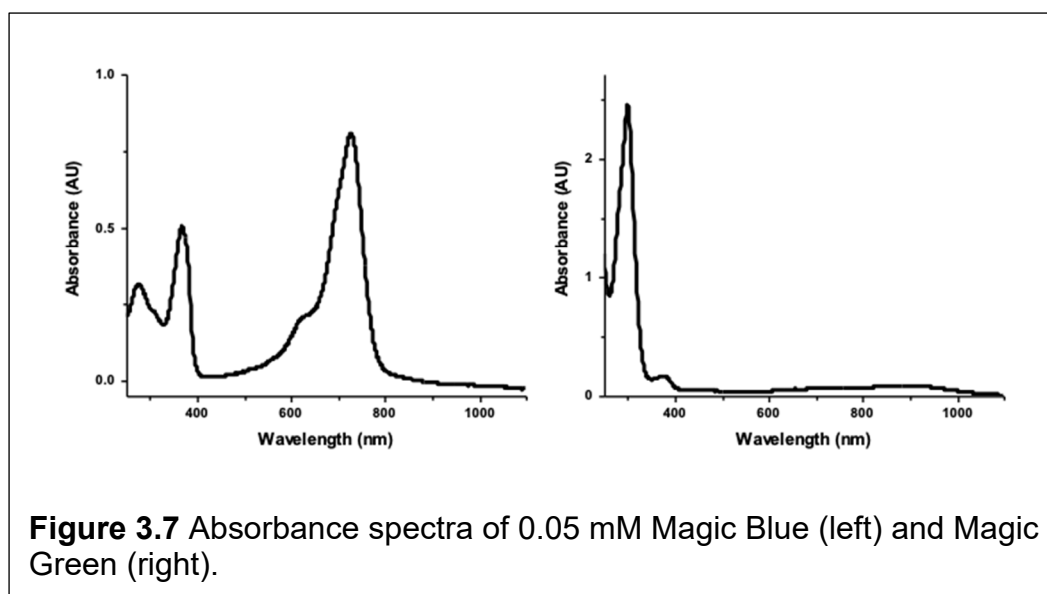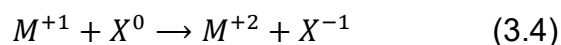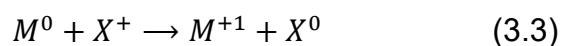
Absorbance spectra of the molecules in the presence of chemical oxidant were collected and optical properties were compared to those of the electrochemically oxidized species. Solutions of $1.5 \times 10^{-3}$ mmol (0.05 mM) **1** in dichloromethane (DCM) with $7.5 \times 10^{-4}$ mmol (0.025 mM) additions of magic blue were prepared, and UV-Vis spectra were collected as shown in Figure 3.4.

The solutions were prepared in a glovebox and capped before being removed from the glovebox for spectral analysis.

**Figure 3.8** Absorbance spectra of 1.5 x 10$^{-3}$ mmoles (0.05 mM) (**1**, a), (**2**, b), and (**3**, c) (DCM) with additions of magic blue. Mole ratios given in the legends are molecule:oxidant.
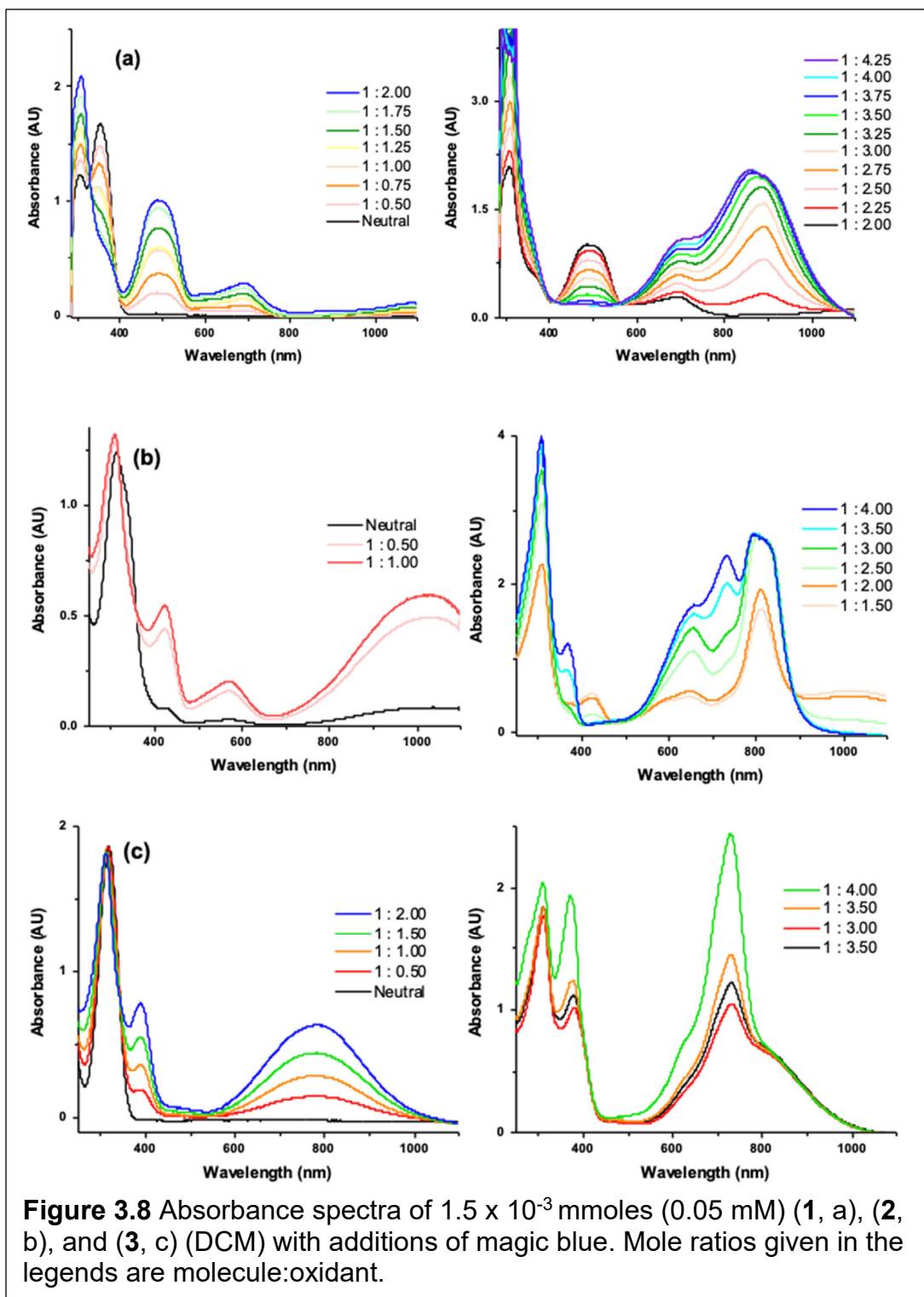
The observed spectral changes in Figure 3.8 for mole ratios of molecule:oxidant ranging from 1.00:0.50 to 1.00:2.25 include increases in absorbances near 301 nm, 500 nm, and 698 nm **(1)**, 420 nm, 560 nm, and 1050 nm **(2)**, and 395 nm and 790 nm **(3)** and decreases in absorbances near 351 nm **(1)** – all relative to the spectrum of the neutral species. The optical properties correspond to those of the first oxidation event observed for the electrochemically oxidized species, so we attributed these changes to the formation of singly oxidized species. As the ratio of magic blue is increased further, the features at 485 nm **(1)** and 420 nm, 560 nm, and 1050 nm **(2)** decreased in magnitude and absorbances near 698 and 876 nm **(1)** and 398 nm, 700 nm, and 810 nm **(2)** were observed, and al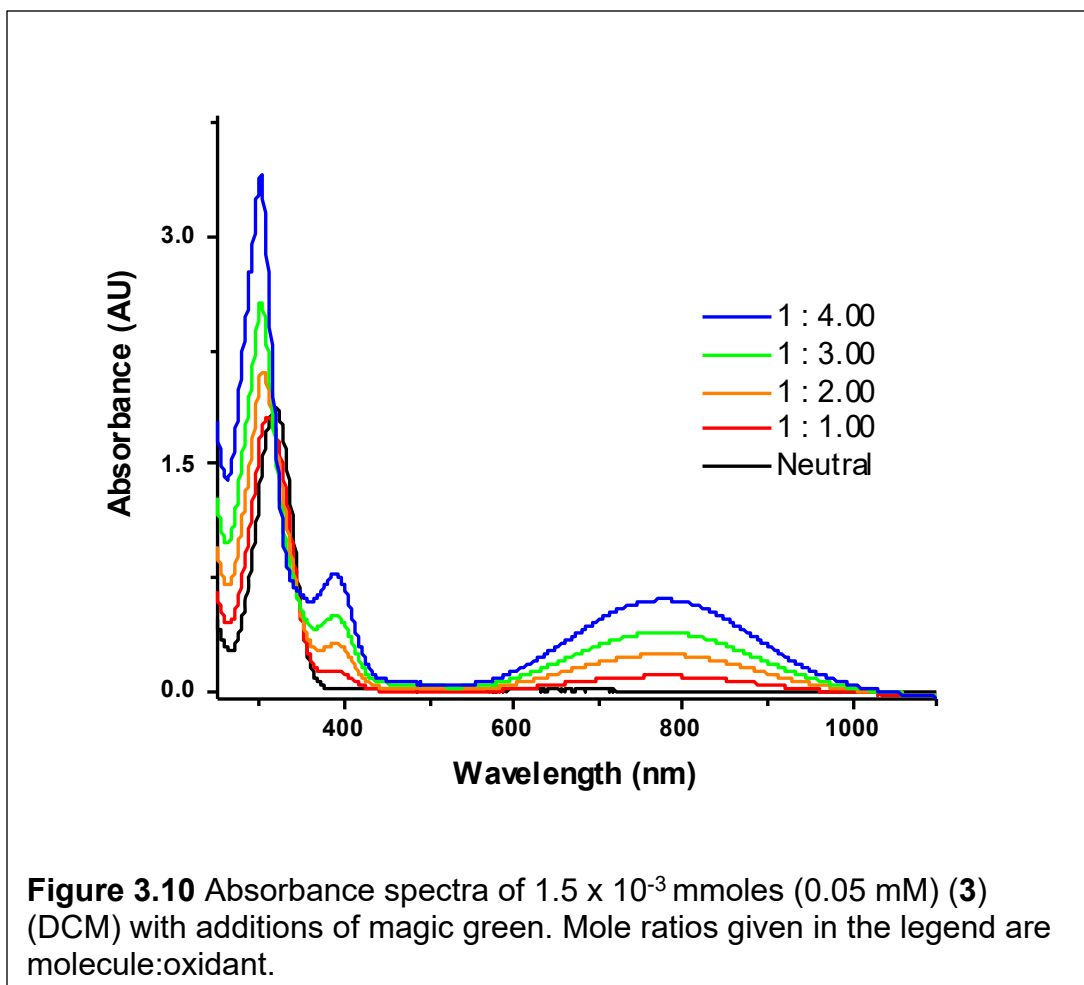l absorbances generally increase in magnitude. These spectral changes correspond to the second oxidation event observed for the electrochemically oxidized species, so we attributed these changes to the formation of doubly oxidized **(1)** and **(2)**.  This data is consistent with disproportionation constants; no spectral evidence for the dication is observed until the amount of chemical oxidant added was sufficient for all molecules to be oxidized once. No new spectral features were observed which implies the molecules are not quickly decomposing.

Characterization of **(3)** with magic blue showed optical properties corresponding to the first oxidation.. As the ratio of magic blue was increased further, spectral features of magic blue were observed and features of the dicationic species did not form. Magic green is a chemical oxidant with more electron withdrawing groups relative to magic blue as shown in Figure 3.9. This stronger oxidant was used to investigate the dicationic optical properties of **(3)**.
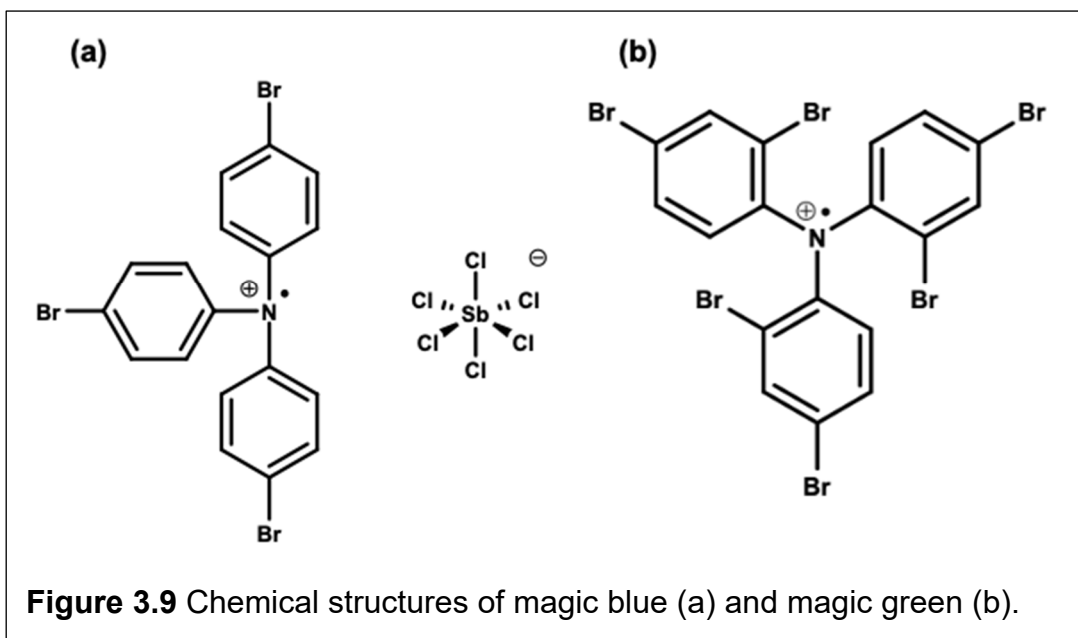
**Figure 3.9** Chemical structures of magic blue (a) and magic green (b).

Solutions of 1.5 x $10^{-3}$ mmol (0.05 mM) **1** in dichloromethane (DCM) with 7.5 x $10^{-4}$ mmol (0.025 mM) additions of magic green were prepared, and UV-Vis spectra were collected as shown in Figure 3.10. The solutions were prepared in a glovebox and capped before being removed from the glovebox for spectral analysis.

**Figure 3.10** Absorbance spectra of 1.5 x $10^{-3}$ mmoles (0.05 mM) (**3**) (DCM) with additions of magic green. Mole ratios given in the legend are molecule:oxidant.

The observed spectral changes in Figure 3.10 for mole ratios ranging from 1:1 to 1:4 include increases in absorbances near 398 nm and 795 nm and decrease in absorbance near 300 nm – all relative to the spectrum of the neutral species. The optical properties correspond to those of the first oxidation event observed for the electrochemically oxidized species, so we attributed these changes to the formation of singly oxidized (**3**). At mole ratios larger than 1:2, a spectral feature near 590 nm was expected to be observed and features of the first oxidation were expected to decrease in magnitude. The cationic species persists, and the second oxidation event observed for the electrochemically oxidized species was not observed. Cyclic voltammetry data suggests (**3**) requires the most energy to oxidize; magic green may not be a strong enough oxidant for the system such that the molecules do not undergo the second

71

oxidation. No new spectral features were observed which implies the molecules are not quickly decomposing. The feature around 318 nm undergoes a bathochromic shift forming a shoulder near the magic green feature at 300 nm which may be attributed to the singly oxidized species converting to the neutral species.

Next, optical changes were monitored over time to monitor the persistence of $M^{n+}$. Because molecules in RFBs could be stored in charged states for long periods of time, time dependence trials are used to qualitatively assess the stability of the charged species. Solutions of varying ratios of the molecules to magic blue were prepared in the glovebox, and UV-Vis absorbance spectra were collected over 24 hours as shown in Figures 3.11-3.13.

**Figure 3.11 Absorbance spectra of 1.5 x 10$^{-3}$ mmoles (0.05 mM) Molecule (1) (DCM) with Magic Blue over 24 hours. Mole ratios are inset and represent molecule:oxidant.**

73
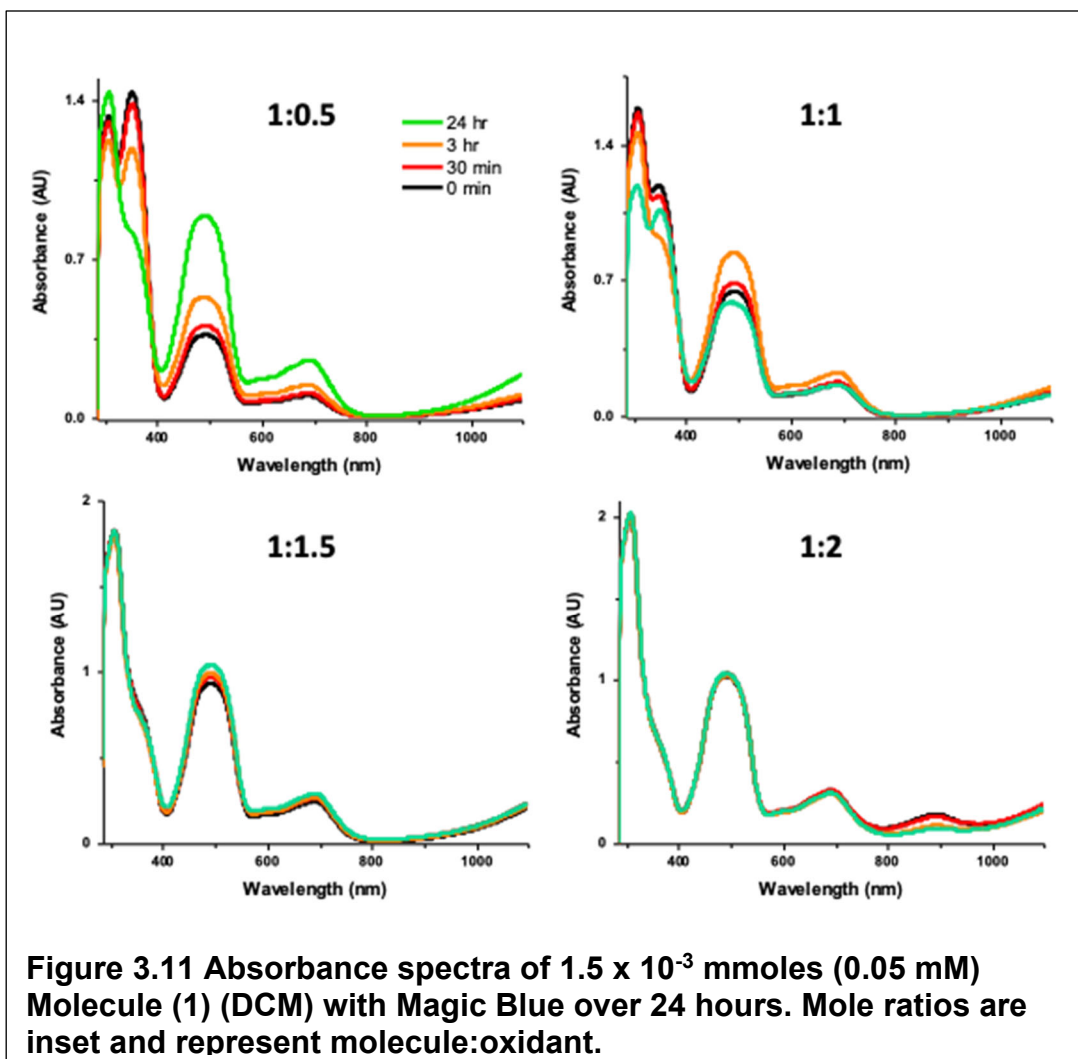
**Figure 3.11 continued**

**Figure 3.12** Absorbance spectra of 1.5 x 10$^{-3}$ mmoles (0.05 mM) Molecule (**2**) (DCM) with Magic Blue over 24 hours. Mole ratios are inset and represent molecule:oxidant.
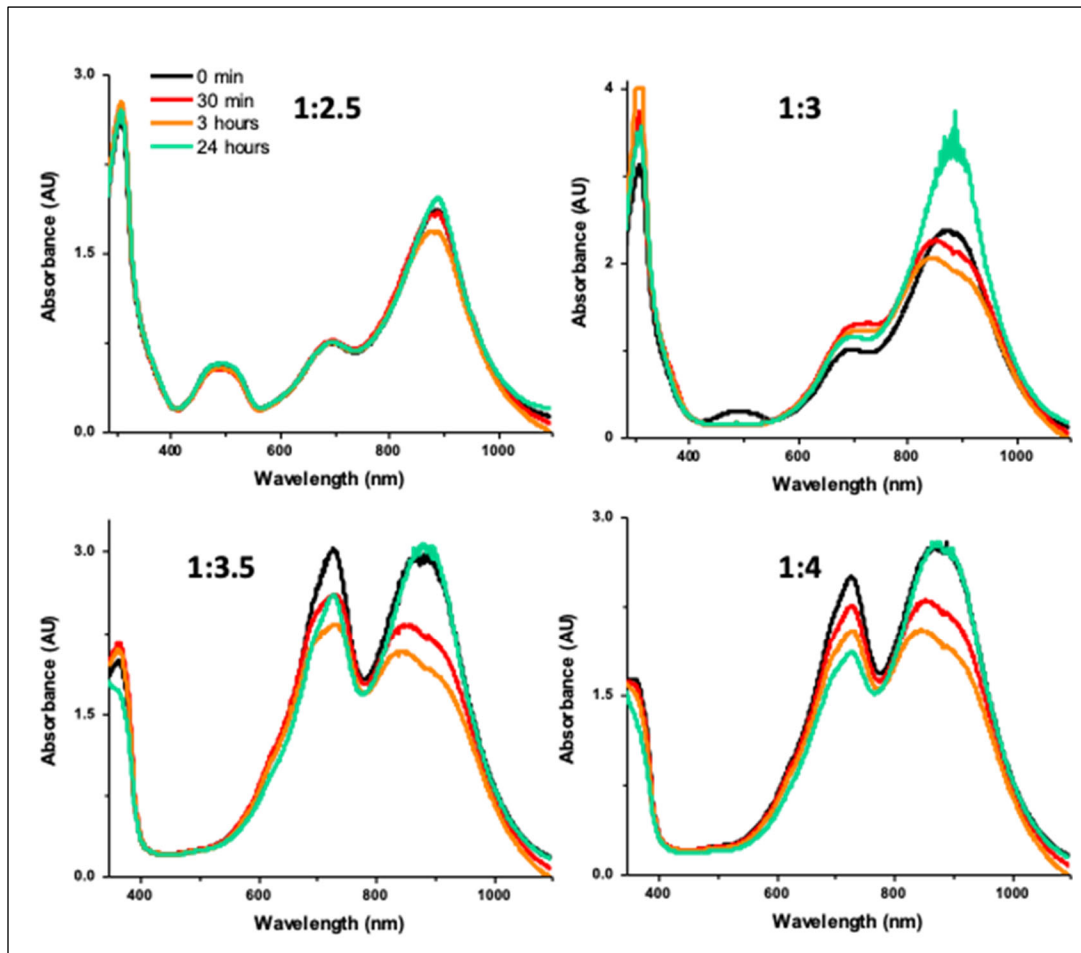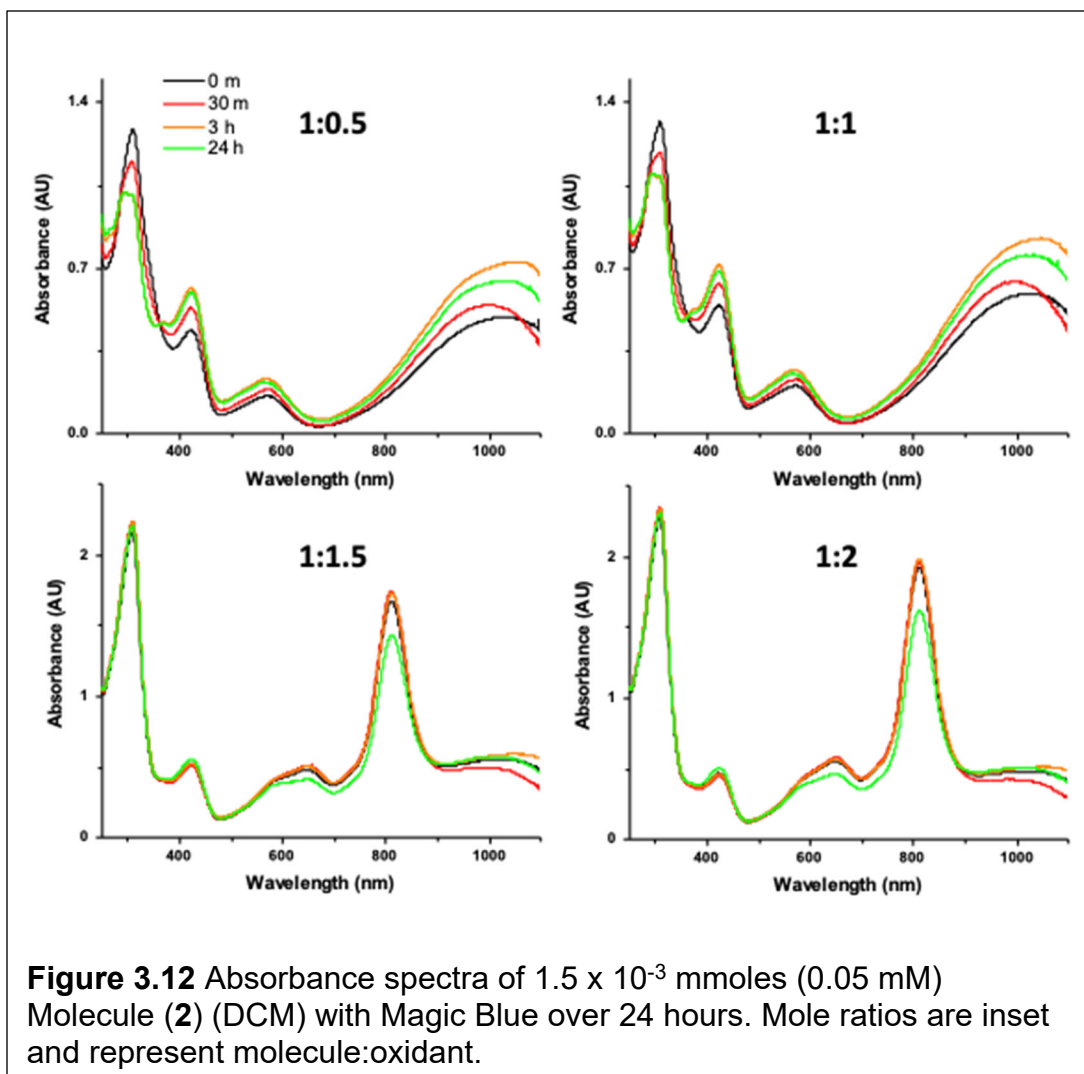
**Figure 3.12 continued**

**Figure 3.13** Absorbance spectra of 1.5 x 10$^{-3}$ mmoles (0.05 mM) Molecule (**3**) (DCM) with Magic Blue over 24 hours. Mole ratios are inset and represent molecule:oxidant.
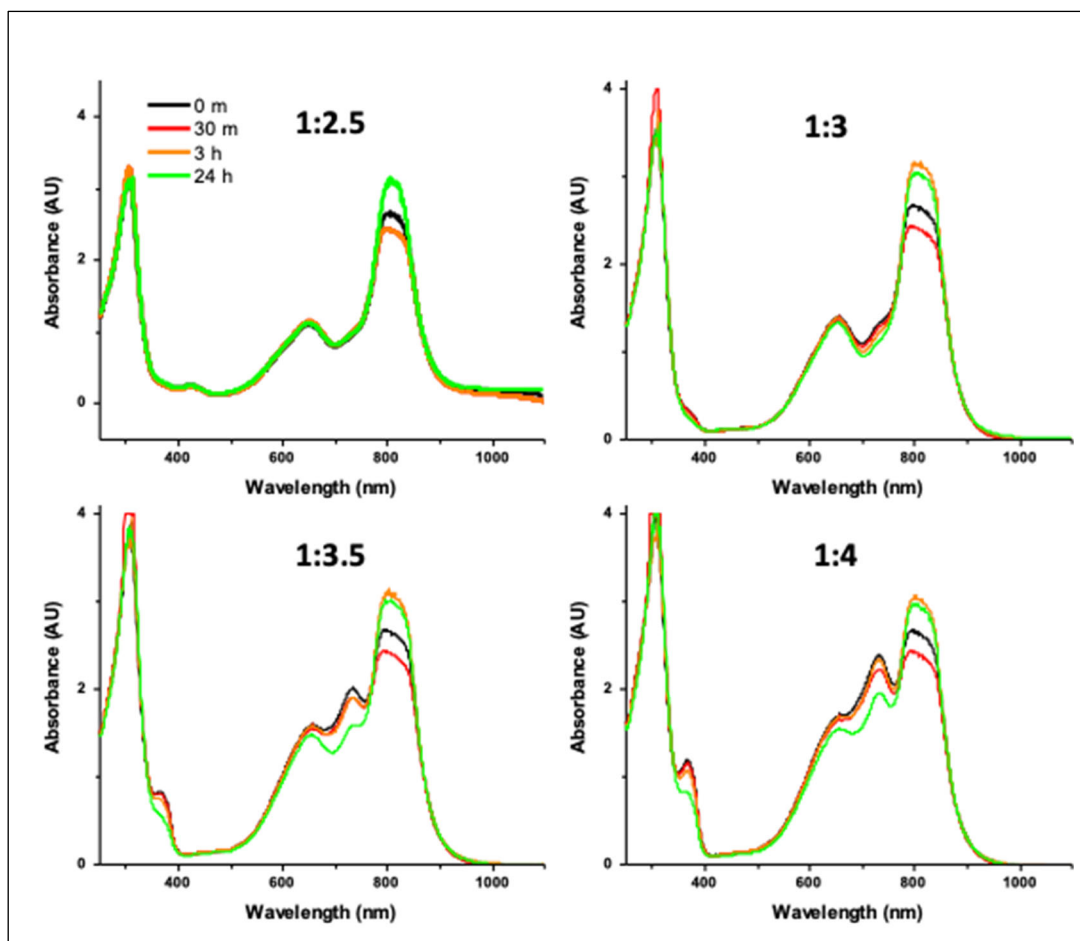
**Figure 3.13 continued**

The observed spectral changes may be attributed to the reaction equilibrium of the $M^0$, $M^{1+}$, and $M^{2+}$ oxidation states over time. If the molecules were fully decomposed, absorbance features associated with the cationic (or dictionic) species would change or new features would be observed. There were no new spectral features observed, further supporting the stability of the charged species, as evidence of decomposition products is not observed. Overall, the spectra qualitatively indicate **(1)** and **(2)** in the cationic and the dicationic species and in the presence of chemical oxidant are stable for short time periods.

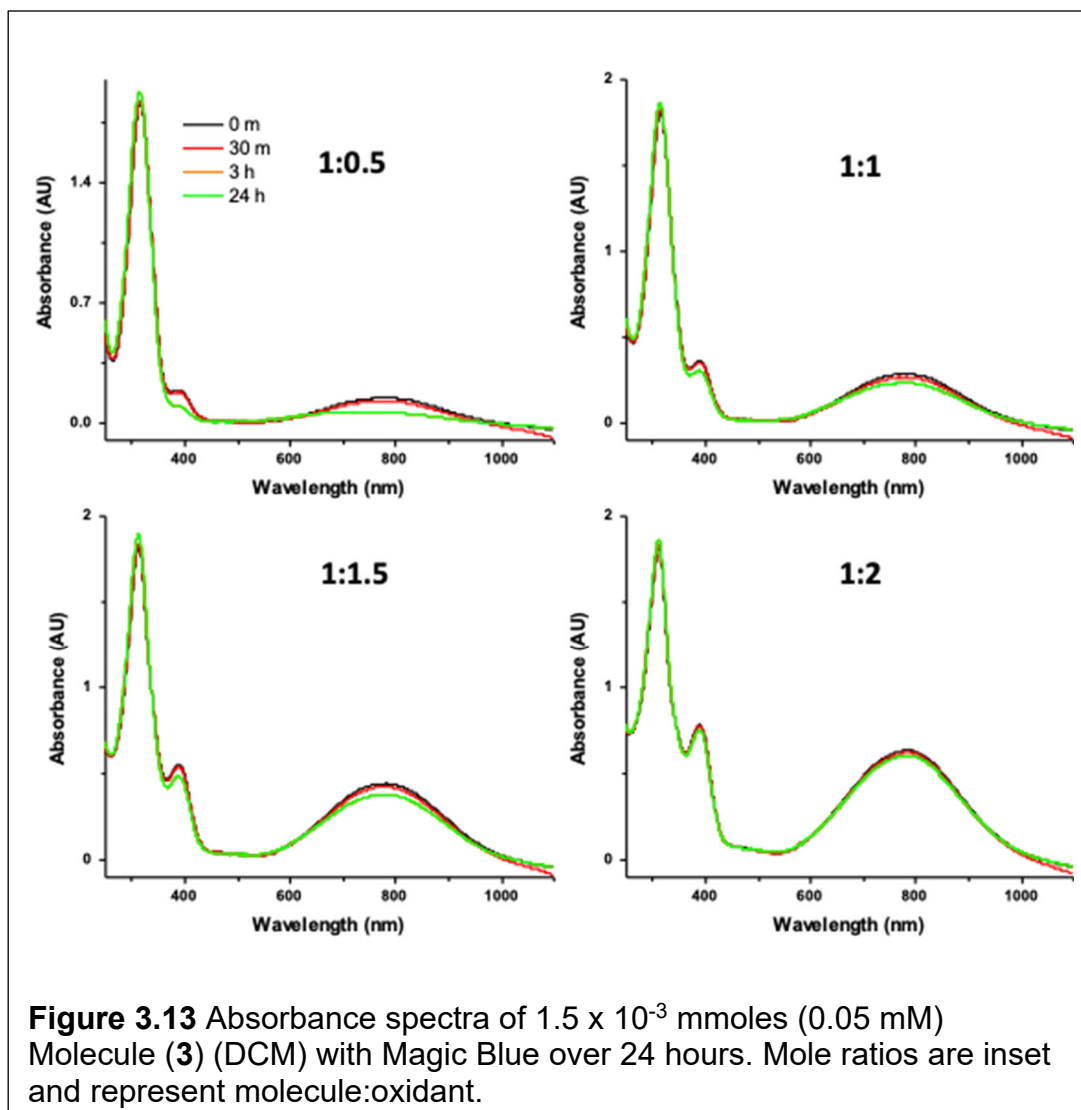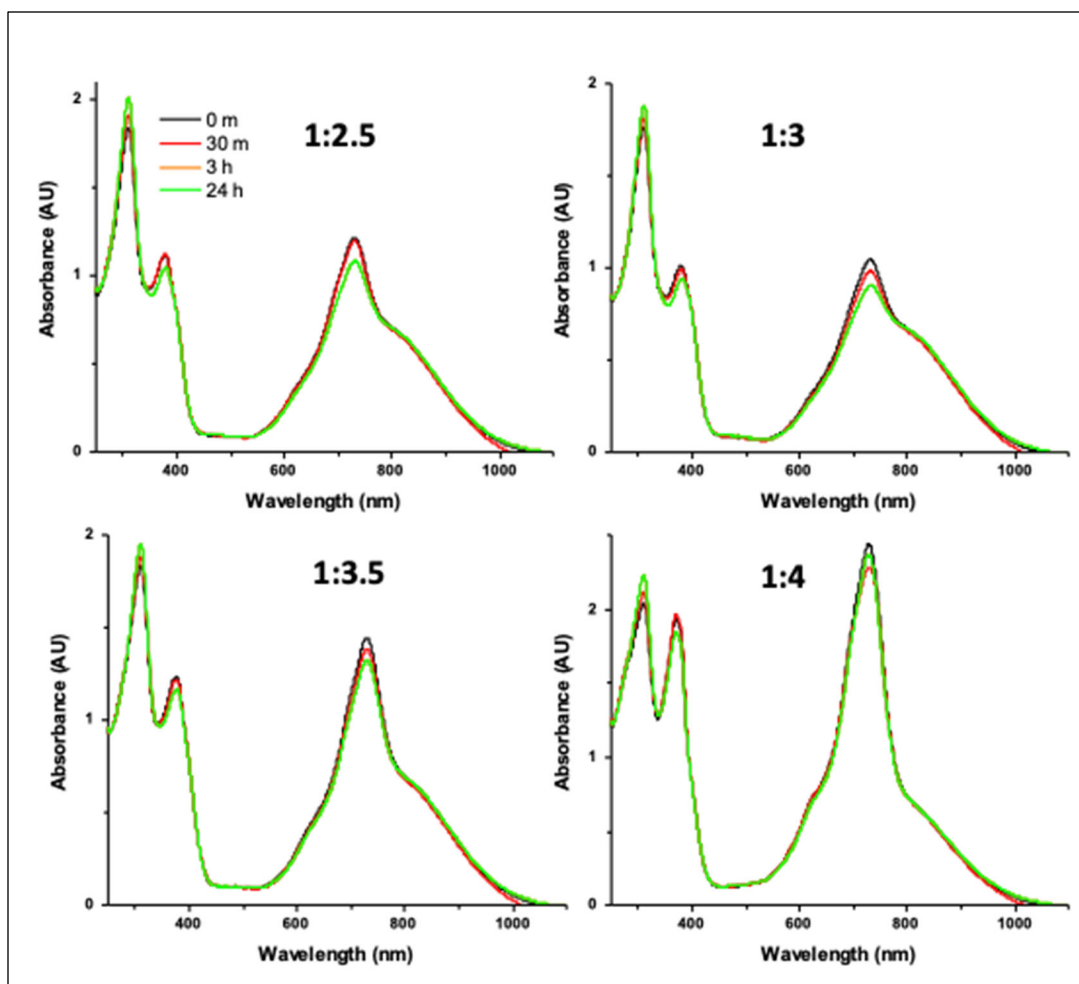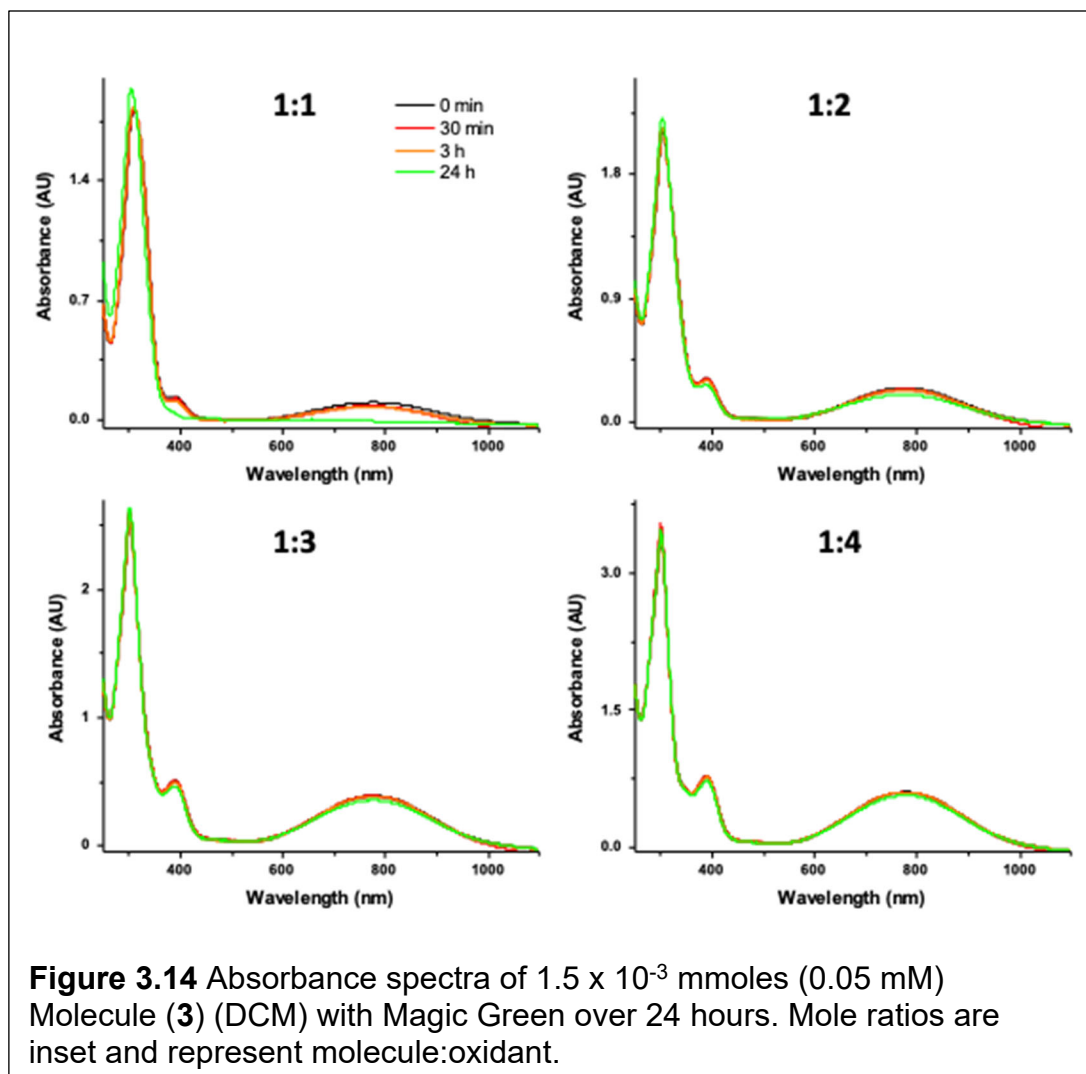The cationic species of **(3)** is observed at ratios 1.0:0.5 to 1:2 in Figure 3.13. As the ratios are increased, cationic features at 395 nm and 790 nm were expected to decrease and a dicationic feature at 590 nm was expected to increase in magnitude. The spectra are dominated by the spectral features characteristic of magic blue and the dicationic features were not observed suggesting the molecule does not undergo a second oxidation.

Optical changes were monitored over time with magic green shown in Figure 3.14. The optical properties of the cationic species for **(3)** form and persist at all ratios of molecule:oxdant. At a 1:1 ratio, the optical properties of the cationic species do not persist beyond 3 hours. There are no new features observed implying the molecules are not decomposing quickly. The observed optical changes may be attributed to the singly oxidized species converting to the neutral species as discussed previously.

**Figure 3.14** Absorbance spectra of 1.5 x $10^{-3}$ mmoles (0.05 mM) Molecule (**3**) (DCM) with Magic Green over 24 hours. Mole ratios are inset and represent molecule:oxidant.

## 3.4 Computational Analysis

  Computational characterization was performed to investigate the degree of electronic communication and delocalization as a function of oxidation. Charge distribution analysis of **(1)** are shown in Figure 3.15. Charge distribution was quantified by investigating the Mulliken charges on each atom. Most of the oxidation charge is carried by the far phenylamine carbons. Charges on side 1 and side 2 differ by the order of a couple thousands of an elementary charge unit which indicates the charge is equally distributed across the molecule. This is supported by the planarization of the biphenyl bridge decreasing as the molecule is oxidized. The neutral molecule has the largest biphenyl central dihedral angle (least planar) and the dication has the smallest angle (most planar). The biphenyl bridge planarizes to allow delocalization as the pi orbitals overlap, leading to charge distribution throughout the molecule.[37] The complete delocalization between the two redox centers places **(1)** in Robin-Day class III. This is supported with cyclic voltammetry; the two redox events are well-spaced and peak separations are large suggesting strong electronic communication.

**Figure 3.15** Change in charge distribution (**1**) with oxidation. Figure provided by Rebekah Duke at the University of Kentucky.
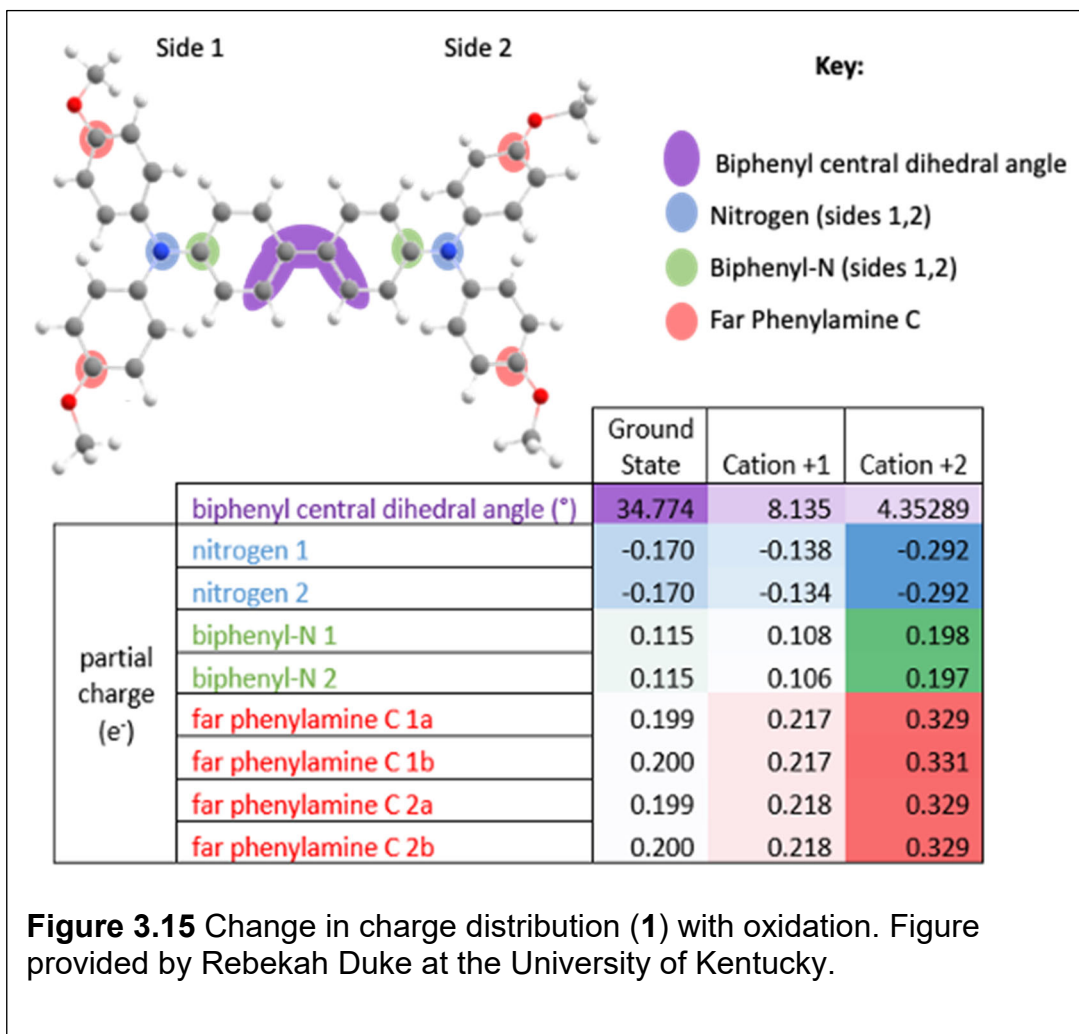
The three molecules investigated underwent two electron-transfer events with clear peak splitting, indicating some level of electronic communication between the redox centers. All molecules have three oxidation states and calculated disproportionation constants indicate comproportionation dominates when the neutral, singly oxidized, and doubly oxidized species are present. The magnitude of ΔE increases from **(1)** to **(3)**. Larger values for **(2)** and **(3)** are a result of the shorter conjugation length relative to **(1).** Molecule **(3)** has the

largest peak splitting due to the addition of an electron withdrawing group, suggesting it requires the most energy to complete the second oxidation.

The spectral features of the cationic and dicationic species are consistent with literature for mixed valence compounds and the neutral, cationic, and dicationic species of each molecule have distinct spectral signatures. The spectral changes due to chemical oxidation of **(1)** and **(2)** agree with those observed for the electrochemically oxidized species. Characterization of **(3)** with magic blue and magic green show optical properties corresponding to the first oxidation. The cationic species persists, however the second oxidation event observed for the electrochemically oxidized species was not observed. Magic blue and magic green may be weak oxidants for this molecule.

The electrochemical oxidation and chemical oxidation data are consistent with disproportionation constants; the singly oxidized species persists until the potential applied or amount of chemical oxidation added are sufficient for all molecules to be oxidized at once. No new features were observed in potential, chemical oxidant, or time dependent trials implying the molecules are not quickly decomposing and are stable for short time periods.

## Chapter 4 Conclusions

  To meet increasing energy needs and mitigate greenhouse gas emissions, energy storage technologies that decarbonize the energy system by storing energy from renewable sources are needed.  RFBs are a modular and scalable energy storage technology that offer design flexibility and can be cost-effectively scaled up. The approach of this research is to utilize low-cost organic redox couples with multiple electron transfers to extend the potential gap, increase output voltage, and improve energy density. This project focused on measuring structure-property relationships in redox-active molecules for use in RFBs.

  The three molecules investigated are promising candidates for applications in RFBs. Electrochemically and chemically oxidized species were found to be stable for short time periods and spectroelectrochemical experiments determined spectral signatures for neutral, cationic, and dicationic species of each molecule that can be monitored to determine the persistence of the species over time. All molecules had well-spaced waves, suggesting all three have some level of electronic communication. Computation data supported these findings as the oxidation of **(1)** was accompanied by a charge shift from the side chains toward the conjugated bridges and planarization suggested delocalization across the bridge.

  The length of conjugated bridges and substituents attached to the bridges induce changes in redox potentials of the molecules which influences the electronic communication mediated by the bridge. Computational analyses of **(2)** and **(3)** will be interpreted in the future to provide more insight into how bridge length and addition of substituents impact molecular geometry and charge distribution.

  In the future, characterization of bis(triarylamines) with varying peripheral substituents and bridge lengths will be completed using a similar procedure.

After the relative stabilities of the molecules are determined, experiments using redox-active molecules in batteries or simulated programs can be completed.

References

(1) Poziot, P.; Gaubicher, J.; Renault, S.; Dubois, L.; Liang, Y.; Yao, Y. Opportunities and Challenges for Organic Electrodes in Electrochemical Energy Storage. *Chemical Reviews* **2020**, *120*, 6490-6557.

(2) Yang, Z.; Zhang, J.; Kintner-Meyer, M.; Lu, X.; Choi, D.; Lemmon, J.; Liu, J. Electrochemical Energy Storage for Green Grid. *Chemical Reviews* **2011**, *111*, 3577-3613.

(3) Weber, A.; Mench, M.; Meyers, J.; Ross, P.; Gostick, J.; Liu, Q. Redox flow batteries: a review. *Journal of Applied Electrochemistry* **2011**, *41*, 1137-1164.

(4) Ibrahim, H.; Ilinca, A.; Perron, J. Energy storage systems - Characteristics and comparisons. *Renewable & Sustainable Energy Reviews* **2008**, *12*, 1221-1250.

(5) Mallick, K.; Das, S.; Sengupta, A.; Chattaraj, S. Modern Mechanical Energy Storage Systems and Technologies. *International Journal of Engineering Research & Technology* **2016**, *5* (2), 727-730.

(6) Harris, C.; Meyers, J. P. Working Smarter, Not Harder: An Introduction to the "Smart Grid". *The Electrochemical Society Interface* **2010**, *19*, 45-48.

(7) Hou, Y.; Vidu, R.; Stroeve, P. Solar Energy Storage Methods. *Industrial & Engineering Chemistry Research* **2011**, *50*, 8954-8964.

(8) Sarbu, I.; Sebarchievici, C. A Comprehensive Review of Thermal Energy Storage. *Sustainability* **2018**, *10*, 191.

(9) Meier, A.; Sattler, C. Solar Fuels from Concentrated Sunlight. 2009.

(10) Soloveichik, G. Flow Batteries: Current Status and Trends. *Chemical Reviews* **2015**, *115*, 11533-11558.

(11) Shoenung, S.; Hassenzahl, W. *Long- vs. Short-Term Energy Storage Technologies Analysis. A Life-Cycle Cost Study. A Study for the DOE Energy Storage Systems Program*; Sandia National Laboratories, 2003.

(12) Amiryar, M. E.; Pullen, K. R. A Review of Flywheel Energy Storage System Technologies and Their Applications. *Applied Sciences* **2017**, *7*, 1-21.

(13) Kim, Y.-M.; Lee, J.-H.; Kim, S.-J.; Favrat, D. Potential and Evolution of Compressed Air Energy Storage: Energy and Exergy Analyses. *Entropy* **2021**, *14*, 1501-1521.

(14) Liu, J.; Chang, Z.; Wang, L.; Xu, J.; Kuang, R.; Wu, Z. Exploration of Basalt Glasses as High-Temperature Sensible Heat Storage Materials. *ACS Omega* **2020**, *5*, 19236-19246.

(15) Winter, M.; Brodd, R. What Are Batteries, Fuel Cells, and Supercapacitors? *Chemical Reviews* **2004**, *104*, 4245-4269.

(16) Chen, R.; Kim, S.; Change, Z. *Redox Flow Batteries: Fundamentals and Applications, Redox*; 2017. DOI: 10.5772/intechopen.68752.

(17) Winsberg, J.; Hagemann, T.; Janoschka, T.; Hager, M. D.; Schubert, U. S. Redox-Flow Batteries: From Metals to Organic Redox-Active Materials. *Angewandte Chemie* **2016**, *56* (3), 686-711.

(18) Dunn, B.; Kamath, H.; Tarascon, J.-M. Electrical Energy Storage for the Grid: A Battery of Choices. *American Association for the Advancement of Science* **2011**, *334* (6058), 928-935.

(19) Li, M.; Rhodes, Z.; Cabrera-Pardo, J.; Minteer, S. Recent advancements in rational design of non-aqueous organic redox flow batteries. *Royal Society of Chemistry* **2020**, *4*, 4370-4389.

(20) Rajarathnam, G. P.; Schneider, M.; Sun, X.; Vassallo, A. M. The Influence of Supporting Electrolytes on Zinc Half-Cell Performance in Zinc/Bromine Flow Batteries. *Journal of The Electrochemical Society* **2016**, *163*, A5112-A5117.

(21) Chai, J.; Lashgari, A.; Jiang, J. Electroactive Materials for Next-Generation Redox Flow Batteries: From Inorganic to Organic. In *Clean Energy Materials*, Vol. 1364; 2020; pp 1-47.

(22) Hu, B.; DeBruler, C.; Rhodes, Z.; Liu, T. L. Long-Cycling Aqueous Organic Redox Flow Battery (AORFB) toward Sustainable and Safe Energy Storage. *Journal of the American Chemical Society* **2017**, *139*, 1207-1214.

(23) Luo, J.; Hu, B.; Hu, M.; Zhao, Y.; Liu, T. L. Status and Prospects of Organic Redox Flow Batteries toward Sustainable Energy Storage. *ACS Energy Letters* **2019**, *4*, 2220-2240.

(24) Wei, X.; Pan, W.; Duan, W.; Hollas, A.; Yang, Z.; Li, B.; Nie, Z.; Liu, J.; Reed, D.; Wang, W.; et al. Materials and Systems for Organic Redox Flow Batteries: Status and Challenges. *ACS Energy Letters* **2017**, *2* (9), 2187-2204.

(25) Ingle, J. D.; Crouch, S. R. *Spectrochemical Analysis*; Pearson College Div, 1988.

(26) Photonics K.K., H. *Photomultiplier Tubes: Basics and Applications*; Hamamatsu Photonics K.K., 2007.

(27) Es'Haghi, Z. Photodiode Array Detection in Clinical Applications; Quantitative Analyze Assay Advantages, Limitations and Disadvantages. In *Photodiodes: Communications, Bio-Sensings, Measurements and High-Energy Physics*, Shi, J.-W. Ed.; IntechOpen, 2011.

(28) Biesheuvel, P. M.; Poranda, S.; Dykstra, J. E. The difference between Faradaic and non-Faradaic electrode processes. *arXiv: Chemical Physics* **2018**.

(29) Zoski, C. G. *Handbook of Electrochemistry*; Elsevier, 2007.

(30) Elgrishi, N.; Rountree, K. J.; McCarthy, B. D.; Rountree, E. S.; Eisenhart, T. T.; Dempsey, J. L. A Practical Beginner's Guide to Cyclic Voltammetry. *Journal of Chemical Education* **2018**, *95*, 197-206.

(31) Products, B. R. *FAQ: EC Electrodes*. https://www.basinc.com/products/ec/faqele#Ref (accessed 2021 January 12).

(32) Bard, A. J.; Faulkner, L. R. *Electrochemical Methods: Fundamentals and Applications*; John Wiley & Sons, INC., 2001.

(33) Khademi, M.; Bard, D. P. J. Structure of the Electrical Double Layer Revisited: Electrode Capacitance in Aqueous Solutions. *Langmuir* **2020**, *36*, 4250-4260.

(34) Sanford, C.; Edwards, M. A.; Klunder, K. J.; Hickey, D. P.; Li, M.; Barman, K.; Sigman, M. S.; White, H. S.; Minteer, S. D. A synthetic chemist's guide to electroanalytical tools for studying reaction mechanisms. *Chemical Science* **2019**, *10*, 6404-6422.

(35) Wang, H.; Sayed, S. Y.; Luber, E. J.; Olsen, B. C.; Shirurkar, S. M.; Venkatakrishnan, S.; Tefashe, U. M.; Farquhar, A. K.; Smotkin, E. S.;

McCreery, R. L.; et al. Redox Flow Batteries: How to Determine Electrochemical Kinetic Parameters. *ACS Nano* **2020**, *24*, 2575-2584.

(36) Bott, A. W. The Study of Multiple Electron Transfer Reactions by Cyclic Voltammetry. *Current Separations* **1997**, *16*, 61-66.

(37) Lambert, C.; Nöll, G. The Class II/III Transition in Triarylamine Redox Systems. *Journal of the American Chemical Society* **1999**, *121*, 8434-8442.

(38) Yurchenko, O.; Freytag, D.; Borg, L. z.; Zentel, R.; Heinze, J.; Ludwigs, S. Electrochemically Induced Reversible and Irreversible Coupling of Triarylamines. *Journal of Physical Chemistry* **2012**, *116*, 30-39.